

Modelling and analysis of crack turning on aeronautical structures

Modelling and analysis of crack turning on aeronautical structures



Doctoral Thesis

Llorenç Llopart Prieto

Director:

Dr. Marc Anglada i Gomila



Company director:

Elke Hombergsmeier



Llorenç Llopart Prieto



Ottoburnn / Barcelona April 2007

2 *State of the art*

This chapter is divided in five sections. The first introduces aeronautical structures and materials and defines the concept of inspection intervals.

The second presents five basic concepts in the fracture mechanics. In particular linear elastic and elastic plastic fracture mechanics are briefly introduced as well as fatigue and the plane strain/plane stress concept. Based on the Linear Elastic Fracture Mechanics (*LEFM*) theory, the importance of the second order term on the William's expansion series, i.e. the *T*-stress, and the necessity of a second parameter to better characterise the stress/strain fields at the crack tip is reported.

In the third section the finite element analysis as well as the process of crack simulation is concisely overviewed.

A review of the existing research on the crack growth and crack turning on aeronautical structures is summarised in the fourth section.

And finally, the current state of development of crack path is reviewed. The crack turning paths are presented, as well as the representatively existing criteria for their assessment. Taking into account the fuselage load conditions, crack growth and turning on aeronautical structures are discussed and the specimens used to this purpose, i.e. the Doubler Cantilever Beam (*DCB*) and the Cruciform Specimen (*CFS*), are presented.

2.1 *Aeronautical structures*

Part of the functions of aircraft structures is to transmit and sustain loads on the different flight phases and during the life of the airplane. Additionally, extern structures provide an aerodynamic function. These requirements are achieved by means of the utilization of thin-walled structures in which the interior surface of the structure is reinforced by longitudinal and transversal stiffening elements. These allow supporting adequately tensions, compressions, flexions and twists without an excessive bulging.

On airplane structures, two main assembly zones can be distinguished: the fuselage and the wing.

The major components of airplane fuselage are curved panels composed of skins and stringers, body frames, floor beams, window frames, and door frames. This are assembled as illustrated in Figure 2.1.

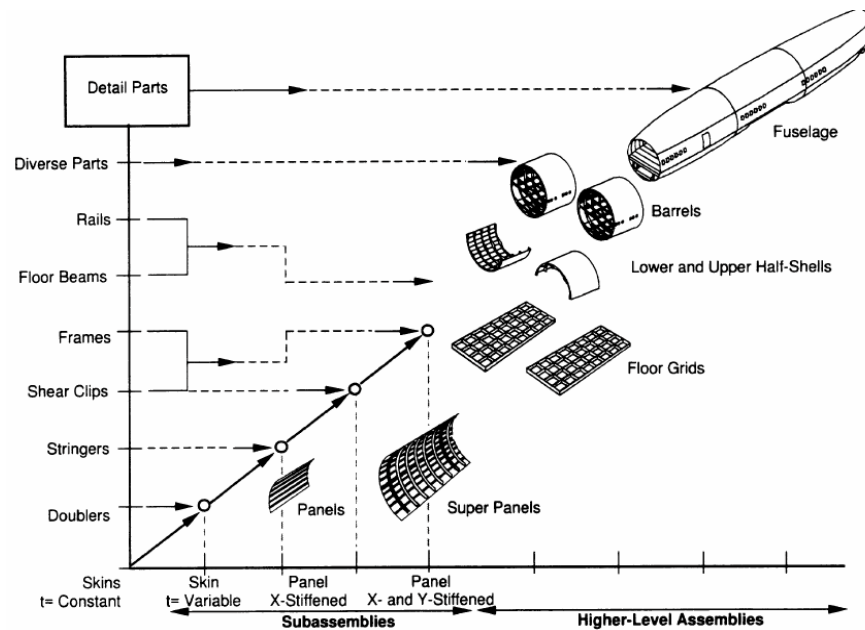


Figure 2.1. Fuselage structure assemblies [1]

The skin is usually made of aluminium alloy with a thickness of few millimetres and it is reinforced with stiffener and frames. Stiffeners, also called stringers, are normally made from extrusions placed on the whole fuselage and joined to the skin. They reinforce the skin providing stability to bending loads, increasing the resistance to bulging and contributing to support traction and compression in the longitudinal direction of the fuselage. Frames are circumferential elements placed perpendicular to the fuselage axis along the whole fuselage. Its fundamental role is to maintain the fuselage cross-section. They are also important to support and transmit different types of loading. As depicted in Figure 2.2, frames transfer payloads into the skins, charging the skins under shear, which at the same time are charged with pressurization loads. It is important to remark that stiffening elements, which essentially provide static strength, are sometimes adequate as skin crack arresters.

Two dimension curved panels are formed by rolling while three dimensional panels are manufactured by stretching.

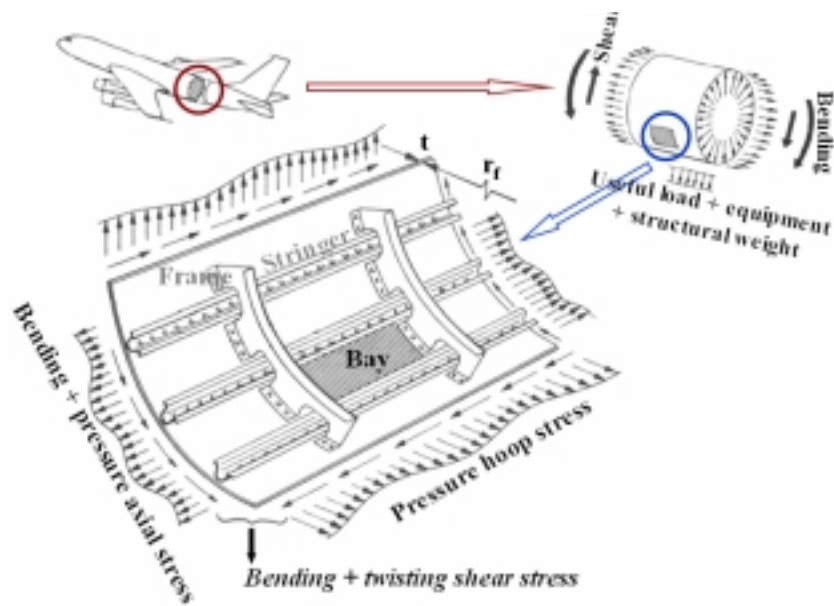


Figure 2.2. Typical fuselage loads

In order to increase the ability of the fuselage to sustain damage caused by fatigue cracking, reinforced doublers, often referred as tear straps, crack stopper straps, or fail-safe straps, depending on its size and shape, are also employed. For example, tear straps are simple strips of material attached circumferentially to the skin of the fuselage. Its role is to arrest an axial crack, which is propagating either sub-critically under fatigue loading or critically after exceeding the fracture toughness.

On the wing, the skins are designed to sustain tensile and compressive loads, and I-, C-beams, called spars, are used for the stability under compressive loads. Chord wire ribs break these spars into short length to increase compressive allowable stresses due to wing bending curvature and they are exposed to air and crashing loads. The skin of the wing is made up of thin sheet of aluminium alloy too. But due to the different conditions on the upper and bottom face of the wing different alloys are used for each side. The generated lifting force makes the wing to flex up, which implies the upper face to work under compression and the lower under traction. The fundamental structural beams of the wing are the spars. They are extended along the wing length perpendicular to the fuselage. Usually, they are two or three on each wing, with a general profile form in “C” or in “T”. Because they are of notable dimensions, they are constructed from the junction of several elements. Finally, the ribs are the elements with the wing profile-form and they are periodically placed parallel to the fuselage [10].

The predominant used joining technique for all these elements on both parts of the airplane is riveting. Nowadays riveting is starting to be substituted by welding to joint different elements on specified parts of the fuselage. Until recently, the welding option was almost discarded because the alloys of major aeronautical interest presented bad weldability in front of traditional methods of joining. Riveted structures and welded/monolithic are called differential and integral structures, respectively. Differential structures present an interface between the skin and the stiffeners, while in integral structures these elements forms one unity with the skin. Both structures are exemplified in Figure 2.3.

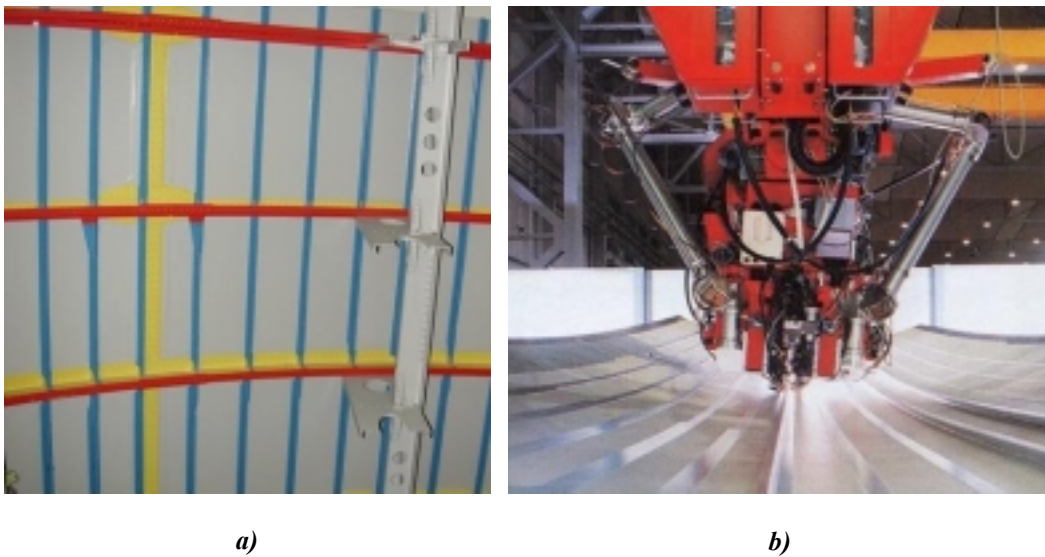


Figure 2.3. a) Differential and b) integral structures [11]

2.1.1 Aeronautical materials

Panels, stringers and frames are made with precipitation hardened Aluminium Alloys (AA). The advantage of aluminium alloys is their lightness, high specific strength and weatherability. The alloys that provide the major mechanical characteristics are *Al-Zn-Mg-Cu*, the 7xxx family, and *Al-Cu-Mg*, the 2xxx family. The two widely used aeronautical alloys are 7075-T6 and 2024-T3. Their weight compositions are described on Tables 2.1 and 2.2.

Table 2.1. Chemical weight composition of the AA 7075-T6 sheet [S1]

Element	Si	Fe	Cu	Mn	Mg	Cr	Zn	Ti	Other		Al
									Each	Total	
Min [Wt%]	-	-	1.20	-	2.10	0.18	5.10	-	-	-	Base
Max [Wt%]	0.40	0.50	2.00	0.30	2.90	0.28	6.10	0.20	0.05	0.15	

In addition, *Al-Mg-Si* alloys, i.e. 6xxx family, are of specially interest. Although they do not have the best mechanical properties, they possess very good behaviour to corrosion and they are weldable.

Table 2.2. Chemical composition of the AA 2024-T3 sheet [S2]

<i>Element</i>	<i>Si</i>	<i>Fe</i>	<i>Cu</i>	<i>Mn</i>	<i>Mg</i>	<i>Cr</i>	<i>Zn</i>	<i>Ti</i>	<i>Other</i>		<i>Al</i>
									<i>Each</i>	<i>Total</i>	
<i>Min [Wt%]</i>	-	-	3.80	0.30	1.20	-	-	-	-	-	Base
<i>Max [Wt%]</i>	0.50	0.50	4.90	0.90	1.80	0.10	0.25	0.15	0.05	0.15	

Extruded profiles have a notable implantation in the construction of aircrafts, e.g. stringers of the fuselage and of the wing, spar and rib cords of the wing, longitudinal and transversal girders (where the panels of the floor for the passengers cabin are placed), rails and tracks (where passenger seats and charge containers are mounted), strengthening elements of bulkheads, transverse watertight sections which separate the pressurized central zone of the cabin with the not pressurized zones and strengthening elements in the rudder [10].

New 7xxx alloys have lower impurities content of iron (*Fe*) and silicon (*Si*), and this improve the fracture toughness. Alloys 7010 and 7050 are more heavily alloyed and for similar thermal treatments they reach higher levels of mechanical properties. Moreover, the substitution of chrome (*Cr*) for zinc (*Zn*) allows the heat treatment of larger sections of the product. On the other hand, the alloying elements will dissolve at the temperature of extrusion, interacting with dislocations and so obstructing the plastic deformation at higher temperatures, making these alloys difficult to extrude. The presence of magnesium (*Mg*) is negative for the extrusion process as well as *Cr*, manganese (*Mn*) or zircon (*Zr*), which precipitate in form of dispersoids, obstructing the process [12].

The alloys 2224, 2324 and 2524 are analogous in composition to 2024, except in the minimum limit of admissible impurities.

In order to improve the mechanical properties of heat-treatable wrought aluminium alloys, thermal treatments are necessary. The thermal treatment specified with T6 is used for the *Al-Zn-Mg-Cu* family and consists of solution and artificial ageing. The T6 treatment provides maximum levels of hardness, elastic limit and resistance to traction, but retrieves modest fracture toughness and induces bad behaviour to corrosion under tensions and cleavage. T7 treatment

consists in a solution and an artificial overageing, which produces a precipitation structure with stable precipitates of large size and more homogeneously spread than the T6 treatment. This overageing treatment decreases the strength and the elastic limit but improves the fracture toughness as well as the corrosion behaviour. On the other hand, T3 consists of a solution heat-treatment followed by cold working and then natural ageing to a substantially stable condition. The T3 treatment improves strength and corrosion behaviour [12].

The most promising family of the new developed alloys to be used on aeronautical structures is the *Al-Li*. These alloys have low density, high elastic modulus and in consequence higher stiffness and they have improved weldability. On the other hand, they have certain limitations regarding plasticity. Thus, it is necessary to apply plastic deformation before artificial ageing. This treatment is specified as T8 condition.

During thermal treatment of all these alloys, important residual stresses are originated after the sudden cooling from the temperature of solution. These residual stresses must be eliminated in order to avoid posterior problems during manufacturing processes or during the life in service. In extruded products, relaxation of residual stresses is achieved by applying a certain quantity of plastic deformation (between 1 and 3%) by means of stretching after solid solution. This application comes specified in the nomenclature by means of the addition of the endings 511 or 510 to the code of the heat treatment [10].

2.1.2 Inspection intervals

Damage tolerance management of aircraft is basically a fourfold problem. First critical locations, stress, corrosion damage, etc. have to be found. Secondly, the loading spectrum of these parts has to be determined. Thirdly, the question of remaining lifetime of the structure according to the first two points has to be answered. Finally, it has to be decided how to manage the component, i.e. inspection intervals, non-destructive evaluations methods and safe life approach [3, 13].

According to the damage tolerance design principles applied to cyclic crack growth in aircraft components, an assumed pre-existing crack must first grow to a given detectable length prior to the first inspection (inspection threshold). This pre-crack can be originated due to manufacturing defects or interpreted as inspection size limit of non-destructive testing methods. The period between the repeated inspections is called inspection interval. These intervals are determined

from the crack growth period between the detectable crack length for the structural detail and the critical crack length under limit load divided by a scatter factor. This scatter factor results from the level of confidence associated to the stress vs. lifetime curve ($S-N$ curve) and to the fatigue stresses applying to the structure. A fatigue scatter factor is defined as the ratio of the mean life to the life for a specified probability of failure and reliability.

More information about the types of aircraft inspection can be found in Table 2.3.

Table 2.3. Types of aircraft inspection [1]

<i>Inspection Type</i>	<i>Purpose</i>	<i>Inspection Interval</i>
<i>Scheduled initial inspections</i>	For accidental damage or other incidents that are outside normal routines	Primarily time dependent
<i>Corrosion prevention inspections (or environmental damage inspections)</i>	Dictated by airline operations and the operations environment, they typically deal with inspecting for and preventing corrosion	Primarily time dependent
<i>Fatigue related inspections</i>	For aging aircraft where a portion (typically 75%) of the design service objective has been reached	Set according to the number of flight cycles an airplane accumulates

2.2 Fracture Mechanics

Fracture mechanics is the analysis of structural behaviour in terms of applied stress, crack length and component geometry. It can be used to establish maximal loadings from a postulated crack length to determine failure of a component while operation, to define critical crack lengths, etc.

A cracked structure can sustain different modes of loading depending on its geometry, orientation of the crack and loading situation. These solicitations can be represented by means of the superposition of three principal loading modes: one tensile opening mode (*Mode I*), and two shearing modes; in-plane sliding mode (*Mode II*) and out-of-plane tearing mode (*Mode III*). These three principal modes are depicted in Figure 2.4.

Because cracked structures are often subjected to a superposition of in-plane and out-of-plane loading, Mixed Mode (*MM*) is defined. *MM* involves that at least two of the fundamental crack modes loading appear occasionally or permanently in combination [14]. This produces an asymmetrical field of stresses and displacements at the surroundings of the crack tip.

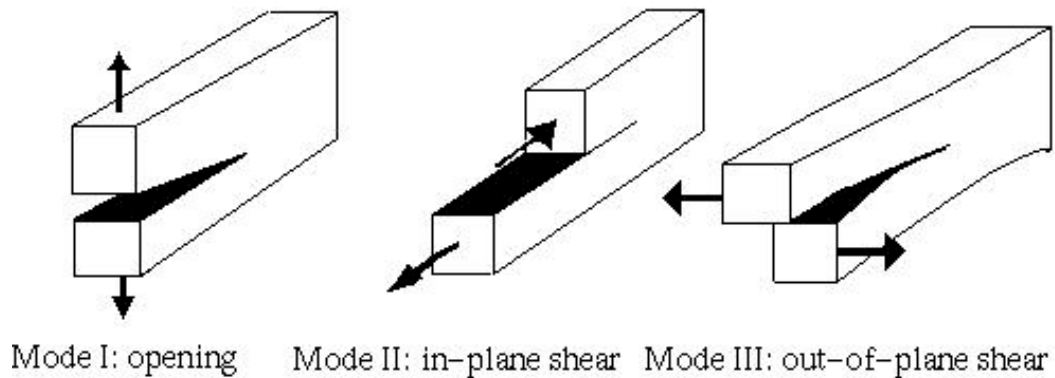


Figure 2.4. The three principal fracture mode loadings

Fracture mechanics theories assume that the state of stresses and strains at the crack tip can be characterised by local parameters representative of the above-defined principal modes of loading. The characterisation can be performed using linear elastic or elastic-plastic theories, which leads to *LEFM* or Elastic Plastic Fracture Mechanics (*EPFM*) respectively [15].

2.2.1 Linear Elastic Fracture Mechanics

Linear Elastic Fracture Mechanics applies when the non-linear deformation of the material is confined to a small region near the crack tip. It assumes that:

- a) the material is homogeneous isotropic continuum, its behaviour is linear elastic, strains and displacements are small and crack surfaces are smooth,
- b) the material is free from large scale self-equilibrating internal stresses and from body forces (gravity),
- c) the analysed domain has a constant thickness,
- d) the initial crack is large (i.e. longer than 1 mm),
- e) loads are applied quasi-statically, and
- f) the growth of a single dominant crack leads to failure [16].

Early works in fracture mechanics, Inglis 1913 [17], were focused on the released energy required to create new crack surface area. Later, Westergaard 1939 [18], Sneddon 1946 [19], Irwin 1957 [20] and Williams 1957 [21] centred *LEFM* on the characterisation of the local stresses and strains in the cracked body.

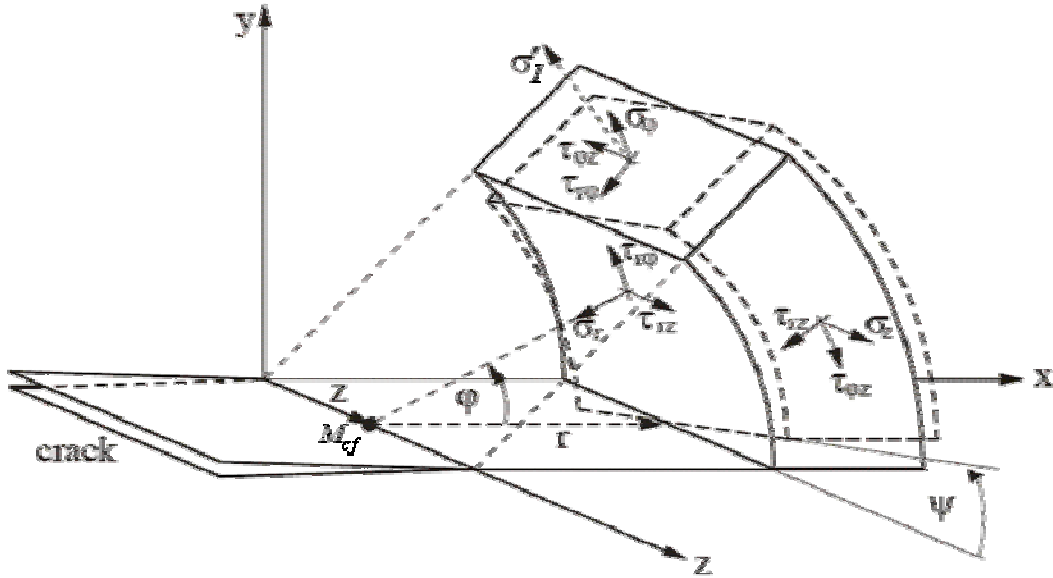


Figure 2.5. Cylindrical coordinate system and stress components at a three dimensional (3D) crack front [22]

Based on the coordinate systems defined in Figure 2.5, Williams [21] characterised mathematically the distribution of the stresses, σ_{ij} , near the crack tip in the *LEFM* domain by means of an expansion series with the contracted form in equation 2.2.1.

$$\sigma_{ij} = \frac{1}{\sqrt{2\pi r}} [K_I f_{ij}^I(\varphi) + K_{II} f_{ij}^{II}(\varphi) + K_{III} f_{ij}^{III}(\varphi)] + T \delta_{ij} \delta_{ij} + O(l) \quad (2.2.1)$$

where K_I , K_{II} and K_{III} are the stress intensity factors (*SIF*) for *Mode I*, *II* and *III* respectively; r is the distance from the crack tip; σ_{ij} are the stresses defined near the crack tip; φ is the polar coordinate angle. $f_{ij}^I(\varphi)$, $f_{ij}^{II}(\varphi)$, $f_{ij}^{III}(\varphi)$ are functions dependent on crack length and geometry, which for a large number of two dimensional (*2D*) crack cases are available on form of diagrams, tables and interpolation formula. These functions are also called the beta or the geometric factors. $O(l)$ represents the contribution of higher order terms on the stress field and T , called the *T*-stress, is an uniform non-singular stress, normal to the crack line and dependent on the type of loading and specimen geometry [23].

In the characterisation of the stress field near the crack tip done by Westergaard, the T -stress was also characterised, but not obtained in a mathematical way. This was added to ensure that the stresses in the crack direction would vanish at infinity [24].

Neglecting the contributions of higher order terms, the developed form of equation 2.2.1, for a 3D cracked body under pure *Mode I* loading, can be written as:

$$\begin{bmatrix} \sigma_{xx} & \sigma_{xy} & \sigma_{xz} \\ \sigma_{yx} & \sigma_{yy} & \sigma_{yz} \\ \sigma_{zx} & \sigma_{zy} & \sigma_{zz} \end{bmatrix} = \frac{K_I}{\sqrt{2\pi r}} \begin{bmatrix} f'_{xx}(\varphi) & f'_{xy}(\varphi) & f'_{xz}(\varphi) \\ f'_{yx}(\varphi) & f'_{yy}(\varphi) & f'_{yz}(\varphi) \\ f'_{zx}(\varphi) & f'_{zy}(\varphi) & f'_{zz}(\varphi) \end{bmatrix} + \begin{bmatrix} T & 0 & T_{xz} \\ 0 & 0 & 0 \\ T_{zx} & 0 & T_{zz} \end{bmatrix} \quad (2.2.2)$$

Assuming plane strain (section 2.2.3), T_{xz} and T_{zx} are zero and $T_{zz} = \nu T$. T was found to increase with the curvature of the crack front when bowing out, but T_{zz} , acting parallel to the crack front, decreases with the crack front curvature [25].

To extend the application domain of the *LEFM* in the direction of higher plastification, the half value of the Irwin plastic zone, r_p , can be added to the crack length [15]. This is calculated under *Mode I* loading as:

$$r_p = \frac{K_I^2}{2\pi R_{p0.2}^2} \nu' \quad (2.2.3)$$

where $R_{p0.2}$ is the yield strength. ν' is 1 for plane stress and $(1-2\nu)^2$ for plane strain. This extension is only applicable when $r_p \ll a$.

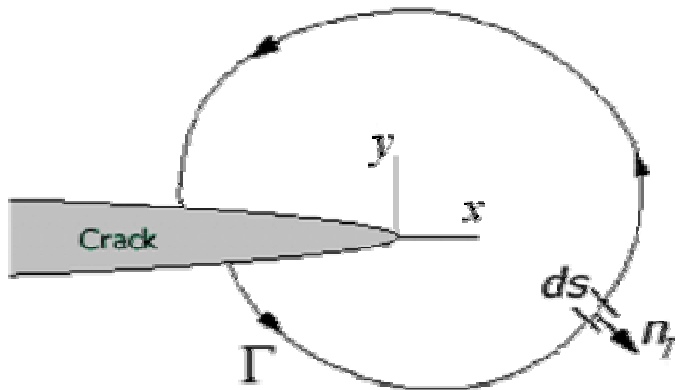
On the other hand, assuming proportional loading and under non-linear elastic behaviour, Hutchinson, Rice and Rosengreen described the stress field based on the Ramberg-Osgood equation derived from the tensile stress-strain curve (*HRR*-approximation) [9, 15, 26, 27].

If the plastic zone in front of the crack is not small compared with crack length and other specimen dimensions, Elastic Plastic Fracture Mechanics is employed to describe crack propagation.

2.2.2 Elastic Plastic Fracture Mechanics

Elastic plastic fracture mechanics applies for isotropic materials with elastic-plastic behaviour. For this purpose, two parameters have been developed: the J -integral proposed by Rice [28] and used principally in the United States, and the Crack Tip Opening Displacement ($CTOD$) suggested by Wells [29] and used widely in Europe. Besides, Shih [30] provided evidence that a unique relationship exists between the J -integral and the $CTOD$ for a given material.

The J -integral evaluates the strain energy release rate of non-linear elastic materials. An important part of this energy is dissipated within the plastic zone. The rest causes the separation of the material. Rice [28] demonstrates that the J -integral is a path-independent line integral which can be written as:



$$J = \int_{\Gamma} \left(w_s dy - T_i \frac{\partial u_i}{\partial x} ds \right) \quad (2.2.4)$$

Figure 2.6. J -integral definition

where $w_s = \sum_{ij}^3 \int_0^{\epsilon_{ij}} \sigma_{ij} d\epsilon_{ij}$ (2.2.4.a) is the strain energy density; $T_i = \sum_{ij}^3 \sigma_{ij} n_{\Gamma j}$ (2.2.4.b) is the traction vector; Γ is an arbitrary contour around the crack tip; n_{Γ} is the unit vector normal to Γ and σ , ϵ , and u are the stress, strain, and displacement fields, respectively.

The J -integral is only computable for monotonic growing strain-stress behaviour.

If the crack tip blunts in the shape of a semicircle, the $CTOD$, also represented by δ , can be defined as either the opening displacement of the original crack tip, or the displacement at the intersection of a 90° angle with the crack flanks as depicted in Figure 2.7. Moreover, the crack

opening can also be characterised using the Crack Tip Opening Angle (*CTOA*) as indicated in Figure 2.7.c, which is directly related with the *CTOD* by means of:

$$CTOA = 2 \tan^{-1} \left(\frac{CTOD}{2l_d} \right) \approx \left(\frac{CTOD}{l_d} \right) \quad (2.2.5)$$

where l_d , illustrated in Figure 2.7.c, is the distance between the crack tip and the *CTOD* measuring point.

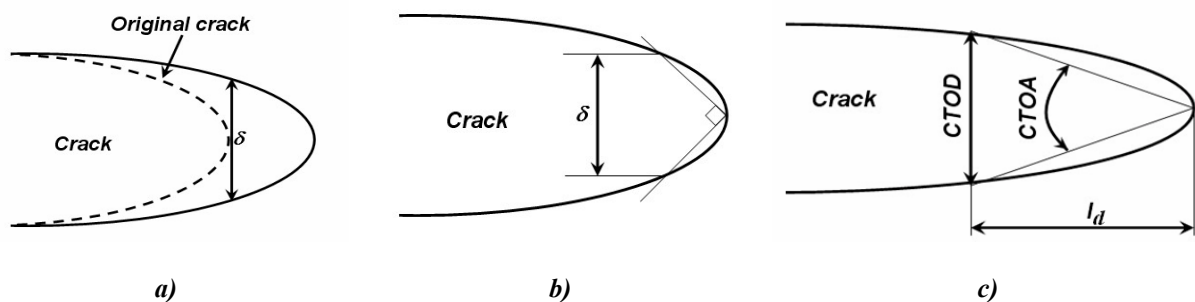


Figure 2.7. *CTOD* and *CTOA* definition

Unstable crack propagation, i.e. structure failure, occurs when the above parameters, defined on both the *LEFM* and *EPFM* domain, reach a critical value, termed K_c , J_c or $CTOD_c$ respectively. Under mixed mode loading the start of unstable crack growth is described by means of a failure curve for plane *MM* and by a failure surface for spatial *MM* load. Figure 2.8 schemes these failure boundaries for the *SIF*.

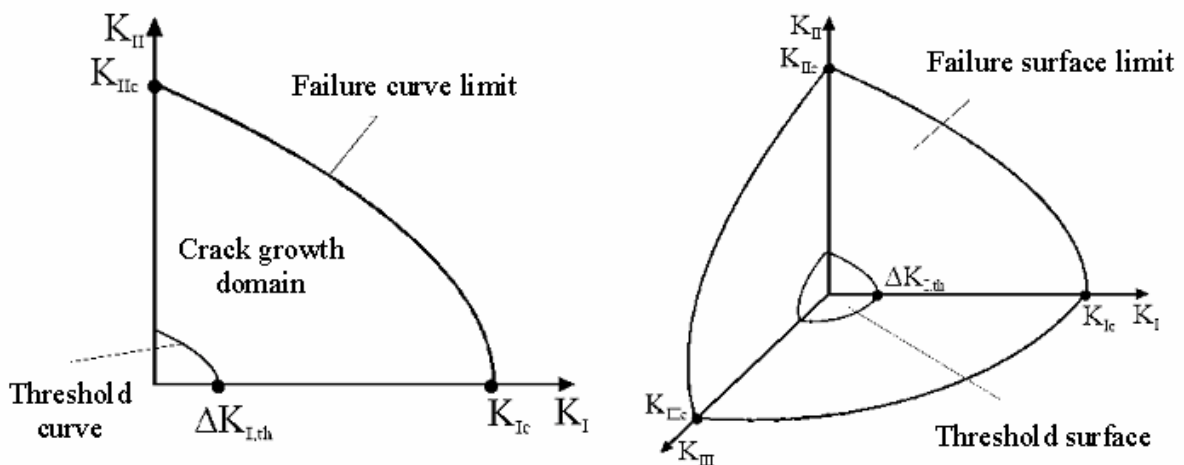


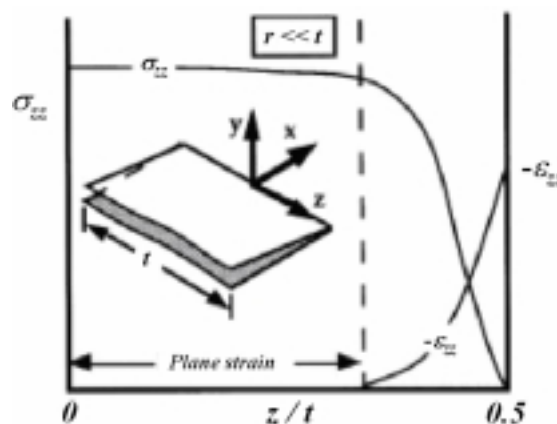
Figure 2.8. K_I - K_{II} and K_I - K_{II} - K_{III} diagrams for plane/surface mixed mode load with failure curve/surface and threshold curve/surface.

2.2.3 Plane strain and plane stress

An undamaged plate loaded in uniaxial tension is subjected to stresses in the plane directions but there is no stress in the thickness direction. It is said that the plate is in a biaxial state of stress. When a *Mode I* crack is introduced, this biaxial state of stress is still present in the bulk of the plate. The material adjacent to the crack tip, highly stressed due to the singularity, is constrained by the surrounding material, which is less stressed. This triggers a Poisson effect along the crack front, causing the material to contract. The surrounding material resists this contraction and the material at the crack front experiences out-of-plane stresses [31].

Because the material at the middle of the crack front is constrained to deform in the thickness direction by the neighbouring material and there is no deformation allowed in this direction so that the strain in this direction is zero. This state is defined as plane strain characterised with a triaxial state of stresses and a biaxial state of strains. As one moves along the crack front from the middle of the specimen thickness to the surface, the constraint decreases. This constrain reduction can be explained with the diminution of the surrounding material. The material at the surface of the plate near the crack tip is not constrained because it is free to deform. Thus, the stress in the thickness direction is zero. This state is defined as plane stress and it is characterised with a biaxial state of stresses and a triaxial state of strains.

This variation on the stresses and strains from the middle of the crack front to the surfaces is depicted in Figure 2.9 for a 3D cracked structure. Since the *SIF* is a characterisation of these stress (strain) fields, a variation on the *SIF* is observed too.



σ_{zz} and ϵ_{zz} are the stress and strain, respectively, in the thickness direction. t is the thickness

Figure 2.9. Variation of stress and strain along a 3D-crack front [31]

2.2.4 The second order term and the two parameter characterisation

In view of the description of the stress fields near the crack tip using the *LEFM*, equation 2.2.1, as r approaches zero, the first term, $1/r^{1/2}$, approaches infinite and the higher order terms remain finite or approach zero. This feature allows characterising the domain at the crack tip with only the first order term in the expansion series of William. For example, Figure 2.10.a depicts the stress distribution normal to the thickness, σ_{yy} , defined on equation 2.2.2. It shows that the stress field in front the crack tip (from red dotted line) can be well characterised by both the full expansion series of Williams (continuous line) and only by the first term (black dotted line).

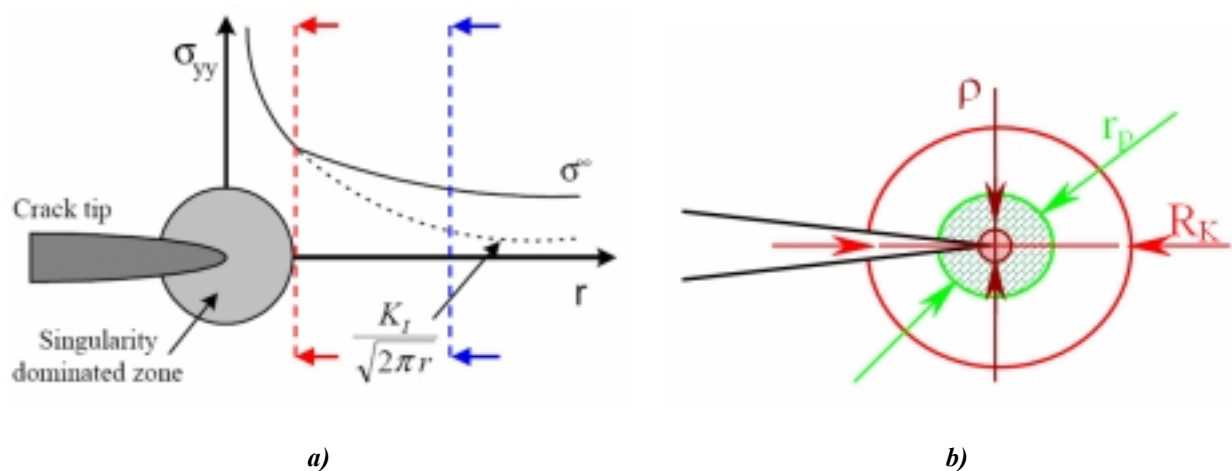


Figure 2.10. Schematic representation of a) stress singularity zone and b) process zone, ρ , plastic zone, r_p , and K -field domain, R_k .

The zone that can be characterised by only the first term is the K -field domain, R_k . Beyond this, higher terms cannot be more neglected. Close to the crack tip, as represented in Figure 2.10.b, there is a region where plastic flow and inelastic deformation takes place. These are the process zone, ρ , and the plastic zone, from ρ to r_p . In these two zones, also called the core region, *LEFM* assumptions are violated, but the general character of the K -field domain in the vicinity of the crack tip is unaffected provided that the size of the core region is limited. The nominal net section stress is used, for example, as indicator of the size of the core region. If this is lower than the 80% of the yield strength the K -field is assumed to be unaffected from the plastification at the crack tip [16, 31].

When characterising the stress field at specific distance from the crack tip, blue line in Figure 2.10.a, the use of only the first term (K_I) is not sufficient and the second order term, T -stress, is also needed.

Furthermore in order to better understand the need of the second order term, an infinite isotropic $2D$ -body containing a crack and loaded to a general state of in-plane modes at its infinitely remote boundaries is considered. Assuming that the material behaviour is linear-elastic the action of the remote loading onto the material at the crack tip should be unambiguously characterized, after the *LEFM* theory, by K_I and K_{II} , i.e.:

$$f_c\left(\frac{K_I}{K_{Ic}}, \frac{K_{II}}{K_{IIc}}, \text{material constants}\right) = 0 \quad (2.2.6)$$

where K_{Ic} and K_{IIc} are the crack toughness for *Mode I* and *Mode II* respectively.

Actually, it is recognized that testing under the above ideal conditions can never take place, because the specimen has a size limit [32]. There will always be some degree of uncertainty whether or not the behaviour can be characterised exclusively in terms of K_I and K_{II} . Therefore, a more relevant description of the crack tip state of stresses may require incorporating higher order terms of the linear-elastic solution.

On the analysis of ductile materials, with both high and small multi-axial state of stress, it was noticed that the description of the crack growth with only the J -integral is not sufficient [26, 33]. This is because the J -integral uniquely controls the intensity of the elastic-plastic crack tip field. There is a series of analytical, numerical and experimental studies, which prove this statement. Pawliska [26] and Zerbst [34], among other authors [27, 35, 36], obtained better characterisation of the stress fields using the J -integral coupled with the T -stress than the J -integral used alone. This is because the approach including the T -stress, gives information concerning how the structural and loading configuration affects the constraint conditions at the crack tip. Moreover, it was seen that the T -stress does not have any influence on the value of the J -integral [37].

Larsson and Carlsson [38], who carried out elastic-plastic finite element analysis of several common cracked specimens by loading them to the same *SIF*, observed different plastic zones, shapes, sizes as well as different crack opening displacements at fixed distance ahead of the crack. They noted that these discrepancies between the different analysed specimens could be reconciled if the elastic stress field includes the T -stress [27, 39].

Other authors [36, 40] noticed that negative T -stresses produce a loss of the HRR -dominance, lower the multi-axial stresses and reduce the hydrostatic stress, which explains also the reduction on crack opening stresses.

Betegón and Hancock [41] concluded that under $2D$ plane strain, positive T -stress signifies the attainment of a single parameter characterisation, while negative T -stress shows the need of a two-parameter description to represent the stress fields.

Some authors were not satisfied with the two parameters characterisation, the SIF or the J -integral with the T -stress, and they proposed other second parameters. Some of them are briefly introduced below.

It is known [42, 43] that the field at the crack tip, where the fracture process can be expected to take place, is a state of stress in which the normal stresses acting on any plane are equal and the shearing stresses do not exist. This state of stress is called the hydrostatic stress. On this basis the triaxiality parameter, Q , was proposed as:

$$Q = \frac{\sigma_{\varphi\varphi} - \sigma_{\varphi\varphi}(HRR)}{R_{p0.2}} \quad (2.2.7)$$

where $\sigma_{\varphi\varphi}$ is the tangential stress and $\sigma_{\varphi\varphi}(HRR)$ is the tangential stress on the HRR -field. This parameter is typically measured at crack tip distance of $2J/R_{p0.2}$ and $\varphi = 0^\circ$. There is a correspondence between the T -stress and the triaxiality parameter Q under small scale yielding conditions. But under continued loading up to full plastic conditions, this relation loses its validity [32]. While the T -stress can be calculated for arbitrary elastic crack configurations, simple and direct methods do not exist to calculate Q .

When using the $2D$ T -stress, a survey of the out-of-plane constraint is not possible, since the T -stress only describes the non-singular stress component in the ligament direction. Therefore, the local stress triaxiality parameter, H , was proposed. This is defined by means of the principal stresses, σ_I , σ_{II} , σ_{III} , normalised by the yield strength, $R_{p0.2}$.

A variation on the definition of H is the use of the von Mises effective stress, σ_e , instead of $R_{p0.2}$, because the ratio σ_h/σ_e has a physical significance for the growth of micro-voids in ductile materials [43].

$$H \equiv \frac{\sigma_h}{R_{p0.2}} = \frac{\sigma_I + \sigma_{II} + \sigma_{III}}{3R_{p0.2}} \quad (2.2.8)$$

Due to the calculation simplicity and independence on the crack tip distance evaluation of the T -stress, the T -stress was used in this work as a second parameter. Beside this it is the most used second parameter in the literature.

2.2.5 Fatigue

Fatigue of metallic materials is a failure mechanism taking place under repeated or cyclic loading. It is composed of crack nucleation and stable propagation until failure. The failure of the structure or the component is produced by the intervention of fracture or gross yielding. Stable crack propagation can be subdivided into two steps of crack growth; micro and macro crack growth. During micro crack propagation, the crack grows along defined slip planes at the interior of the component. This growth depends on grain size and orientation and the presence of inclusions. The growth of a macro crack follows a macroscopic not crystallographic plane usually perpendicular to the applied loading.

An idealized plot, for a given mean cyclic stress, of a typical relationship between the SIF -amplitude, ΔK , and the crack growth rate for a metal, da/dN , is depicted in Figure 2.11.

In region I, crack growth can be retarded completely, if the SIF -amplitude lay below an amplitude threshold, ΔK_{th} . Region II is characterised by a linear growth on the double logarithmic scale (log-log). In region III, the maximum applied stress intensity factor approaches the material toughness, and the crack growth rate accelerates until failure. The crack growth curve is dependent on the stress ratio, R . As R increases, the crack growth rate tends to increase with.

Paris [44] proposed the first law for crack growth which exploits the observed behaviour in region II that is:

$$\frac{da}{dN} = C_p (\Delta K)^{n_p} \quad (2.2.9)$$

where C_p and n_p are constants that can be found by a curve fit to experimental data. C_p is dependent on the tested stress ratio. Because for many components region II represents the major part of the fatigue life, the Paris law has been widely applied and it is usually used when a large amount of test data are not available.

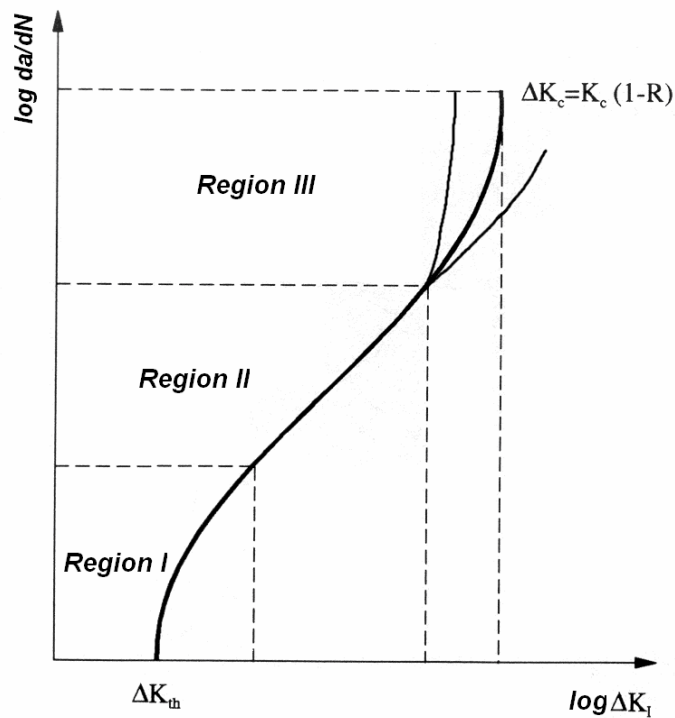


Figure 2.11. Idealized plot of SIF-range and crack growth rate for a metal at a given mean cyclic stress

Forman [45] developed the Paris law further to take into account the effect of the stress ratio and the acceleration produced when the SIF approaches the fracture toughness, i.e. describes region III too.

$$\frac{da}{dN} = \frac{C_f (\Delta K)^{n_f}}{(1-R)K_c - \Delta K} \quad (2.2.10)$$

where C_f and n_f are constants that can be found by a curve fit to experimental data and K_c can be evaluated after the ASTM E399 test [S3]. Since damage tolerance in aircraft structures generally evaluates a structure containing an existent damage, region II is of most importance. For that reason, this law is extensively used when analysing aeronautical structures.

The whole crack growth curve in Figure 2.11 can be represented, among others, with the so-called Forman-Newman-deKoning law, which includes the retardation produced near the threshold amplitude, ΔK_{th} . This law has the form in equation 2.2.11.

$$\frac{da}{dN} = \frac{C'(1-f_F)^{n_p} \Delta K^{n_p} \left(1 - \frac{\Delta K_{th}}{\Delta K}\right)^p}{(1-R)^{n_p} \left(1 - \frac{\Delta K}{(1-R)K_c}\right)^q} \quad (2.2.11)$$

where C_f , C' , n_p , p and q are empirical constants; n_p is the same constant as in the Paris law and f_F is a function that incorporates the effect of crack closure under constant amplitude loading, R_c . The definition of the function f_F is described in reference [46].

However, there are several constants in the Forman-Neuman-deKoning law and its sub-functions, which have to be determined through empirical tests. *NASA* has performed over 300 different material and environment combinations tests in order to determine these constants. This information has been incorporated into the NASGRO[®] and FRANC3D[®] tools.

Another law which describes the whole curve of crack growth is the SINH Model. This model is based on a hyperbolic sine function, and it can be written down as:

$$\log\left(\frac{da}{dN}\right) = B_1 \sinh(B_2(\log(\Delta K) + B_3)) + B_4 \quad (2.2.12)$$

B_1 , B_2 , B_3 and B_4 are empirical constants, which must be determined for a given stress ratio, R .

When regarding different crack growth rate curves from experimental tests on the same material system, it is often found large scatter in the results, which can not be accounted for by experimental errors in the measurements. This scatter is essentially due to the random nature of

fatigue crack growth, which is a consequence of the non homogenous structure of real materials. This scatter is then intrinsic to fatigue crack growth measurements.

2.3 Numerical methods

Analytical engineering techniques reach their limitation when evaluating the exact behaviour of complex loaded structures. In the late forties a numerical technique was developed to be used in structural analysis to solve boundary value problems: the finite element analysis (*FEA*) or *FEM*. The *FEM* operates on the assumption that any continuous function over a global domain can be approximated by a series of functions operating over a finite number of small sub-domains. In its application, the object or system is represented by a geometrically similar model consisting of multiple, linked, simplified representations of discrete regions, i.e. finite elements. Equations of equilibrium, derived from applicable physical considerations such as compatibility and constitutive relations, are applied to each element, and a system of simultaneous equations is constructed. The system of equations is solved for unknown values using the techniques of linear algebra or nonlinear numerical theories.

In the 80's another methodology was developed, the *BEM* which operates similar to *FEM*. The *BEM* is becoming more used in many engineering disciplines as an effective alternative to the *FE*-method, because it requires calculating only boundary values rather than values throughout the space defined. This reduces the dimensionality of the problem. *BEM* requires a substantial reduction in data preparation and a much smaller system of algebraic equations to be solved. On the other hand, the system of equations generated by the *BEM* is fully populated and non-symmetric, thus the required computational time can become large for complex structural models, but *BEM* is often more economical, because the model can be split into smaller simpler sub-models. These small parts are modelled and computed independently and then the solutions are joined together along an interface [47, 48].

Meshes can be constructed of either triangular/pentahedral or quadrilateral/hexagonal elements, or combination of both on *2D*- or *3D*-models, respectively. The evaluation of a variable field, U' , inside the element is solved by the use of the shape functions, N_i . These calculate the field variable at other locations of the element from known values, U'_i , on the nodal or integral points, equation 2.3.1.

$$U' = N_1U'_1 + N_2U'_2 + \dots + N_iU'_i + \dots + N_nU'_n \quad (2.3.1)$$

These functions can be seen as a polynomial interpolation over an element. The most used are Lagrange linear function, quadratic or cubic and Hermite cubic function. A representation of such shape functions are shown in Figures A.1 and A.2 in the annexes. The characteristic of these functions is that they have a value equal to 1 at its associated node and 0 at the other nodes. Therefore, the coefficient multiplying a shape is the actual value at a node and the sum of all shape functions at any position is always 1. Based on the polynomial interpolation degree of the shape functions, two different concepts can be defined inside the *FE*-method: the h-element method, which use a polynomial interpolation degree of 1, or 2, and the p-element method, which consists to elevate the polynomial degree, i.e. the interpolations order from the shape functions, until the 8th, 9th or 11th order [49-51].

The accuracy level of the results of simulation techniques depends on the mesh size for the h-element method and on the polynomial degree of the interpolation for the p-element method. Consequently, on the finite p-element method, the description of the geometry has to be independent of the quantity of elements, and the constructed elements should represent the boundaries of the component [52].

2.3.1 Crack growth simulation

The process of crack growth simulation is an incremental one, where a series of steps are repeated for a progression of models. This is formed by three primary collections of data, or databases, which are required for each iteration, i.e. the representational database, R_{di} , the stress analysis database, A_{di} , and the equilibrium database, E_{di} , where i represents the iteration or increment number.

First, the database is represented with an unambiguous description of the cracked body, i.e. solid model geometry, applied tractions, displacements, body forces and materials constants. The representational database is transformed by a discretisation to a stress analysis database, A_{di} . This includes a series of nodal points, where primary field variables are computed or prescribed, a mesh connecting these points, a specification of known conditions at the nodal points, material state and constants, and information necessary to compute body forces, stresses and strains. A solution procedure is used to transform the analysis database to an equilibrium database, E_{di} ,

which consists of primary loads and displacements and secondary stress and strain field variables that define an equilibrium solution for the model analysis.

The equilibrium database should contain field variables and material state information for all locations in the body. These values may be stored explicitly at nodal or integration points, or evaluated using interpolation or extrapolation. In the context of the crack growth simulation, the equilibrium database will also contain values for the stress intensity factors, or other fracture parameters like the T -stress, at all points along all crack fronts. E_{di} is then used in conjunction with the current R_{di} to create R_{di+1} [50, 51, 53].

The crack turning simulation route, on both quasi-static and cyclic crack in plane problems under proportional loading, follows a procedure that treats the action of crack curving on the basis of repeated straight line crack propagation with changing direction. The calculation of this direction is performed following a crack turning criterion [33].

Energy release rate and displacement compatibility methods can be used to calculate crack tips stress intensity and stress concentration factors necessary for the damage tolerance design of structures [5]. Other methods to calculate the stress intensity factor can be found in the literature, for example the standard domain integral method, the interaction integral method (*IINT*), the virtual crack extension method, the virtual crack closure integral method (*VCCI*) [54] and local methods. Local methods are more strongly dependent on the local field at the crack tip than energy methods. Besides, the integral methods have the advantage that the calculation method is path independent, e.g. through the J -integral, but they need a high programming effort. On the other hand, local methods derive the K -factors from either the displacement or stress field at the crack tip, and thus they take into account all applied loadings and constraints.

The different SIF calculation methods have shown to be enough accurate to be used on *FE*-codes. A big number of codes use the local method because of its programming simplicity. In general, the codes that use energy methods have implemented the interaction integral method, which calculates the K -factors by means of the J -integral.

Similarly to the calculation of the stress intensity factor, the T -stress can be computed by means of different methods, for example by the stress substitution method, the Leever & Radon variation method [55], the Eshelby J -integral method applied by Kfoury [56], the weight function

method from Sham [37], the interaction integral method [57], the line spring method from Wang and Parks [33] and by the method based on the Betti-Rayleigh reciprocal theorem [57, 58].

2.4 Crack path

At the present state of the art the factors controlling the path taken by a propagating crack are not entirely understood. Usually, it is assumed that the crack path is known, either from theoretical considerations, or from the results of laboratory tests. At the first stages of the studies it was assumed that crack turning took only place if there was a combination of minimum two modes of loading and the crack turning angle is dependent on the shear portion of the loading.

However, under *Mode I* loading, stable tearing test results showed that crack turning takes place on a relatively short distance from the crack tip. This phenomenon was attributed to geometric imperfections, which would give rise to small amounts of K_{II} at the end of a notch or a crack. These imperfections or perturbations could result from manufacturing imperfections in the specimen geometry, effects of gravity on the specimen, and natural meandering of the crack tip due to material inhomogeneity [8, 9].

These inhomogeneities increase the stress and strain localization around them. If the perturbation of the stress/strain fields are near the crack tip, necking, dimpling or/and other mechanisms such as void growth between these two positions (crack tip and perturbation site) can occur. The stress field in the vicinity of the onset point of the strain localisation will decide the future path of the crack. The symmetric axis of the specimen is abandoned by crack turning. From this moment on, the future path should be more predictable since the asymmetry is larger compared to random perturbations and K_{II} mode is generated.

Because the key point for crack turning under *Mode I* loading is not situated directly near the crack tip, the characterisation of the stress/strain fields at the crack tip must include the second order term, the T -stress.

2.4.1 Rotation of the crack surface

Due to in-plane and out-of-plane loading, the crack surface can experiment a turn in one or two different angles, φ_c and ψ_c , as illustrated in Figure 2.12. If the initial crack is in mixed *Modes I*

and *II* there is a kink at a *Mode I* branch crack. For mixed *Modes I* and *III* a twist is produced and for a combination of all three loading modes a mix of the two turning angles is observed.

Moreover, in reference [59] it has been observed that materials without geometric constraints (e.g. welded seams), with certain ductility at failure and loaded under mixed mode loading might fail by two distinctively macroscopic fracture types, i.e. opening and shear. As illustrated in Figure 2.13, at the crack tip and perpendicular to the loading direction, the maximal hydrostatic stress is developed and the crack initiation and propagation takes place by microvoid coalescence in the direction of the maximum tensile stress. Furthermore, the shear failure takes place at the direction of the maximal shear load. This corresponds where local gliding occur which drive the local strains to failure [27]. These engender the crack to deform asymmetrically as shown in Figure 2.13.

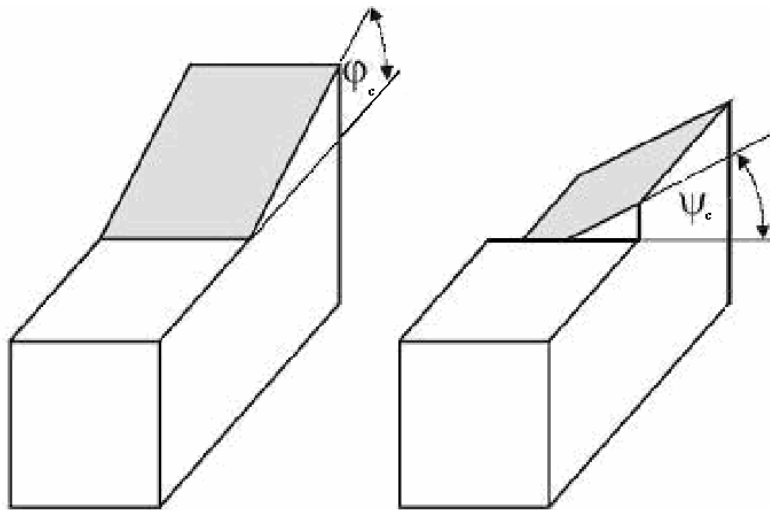


Figure 2.12. a) Turning angle ϕ_c under plane mixed mode loading. b) Twist angle ψ_c under overlay *Mode I* and *Mode III* loading [14]

Even though, shear crack growth is usually associated to static loads there are some situations where shear dominated crack growth takes place under cyclic loading in a homogeneous and isotropic material:

- a) in shear bands at the initial crack tip, where stress levels are low.
- b) when the net section stresses approach or exceed the shear yield strength,
- c) when a static compressive stress is applied or,

- d) when the cyclic stress has a large compressive component,
- e) in the presence of a geometric constraint, and
- f) under some types of out-of-plane loadings [16].

Under the first conditions, stress levels are high, and therefore *LEFM* is not applicable.

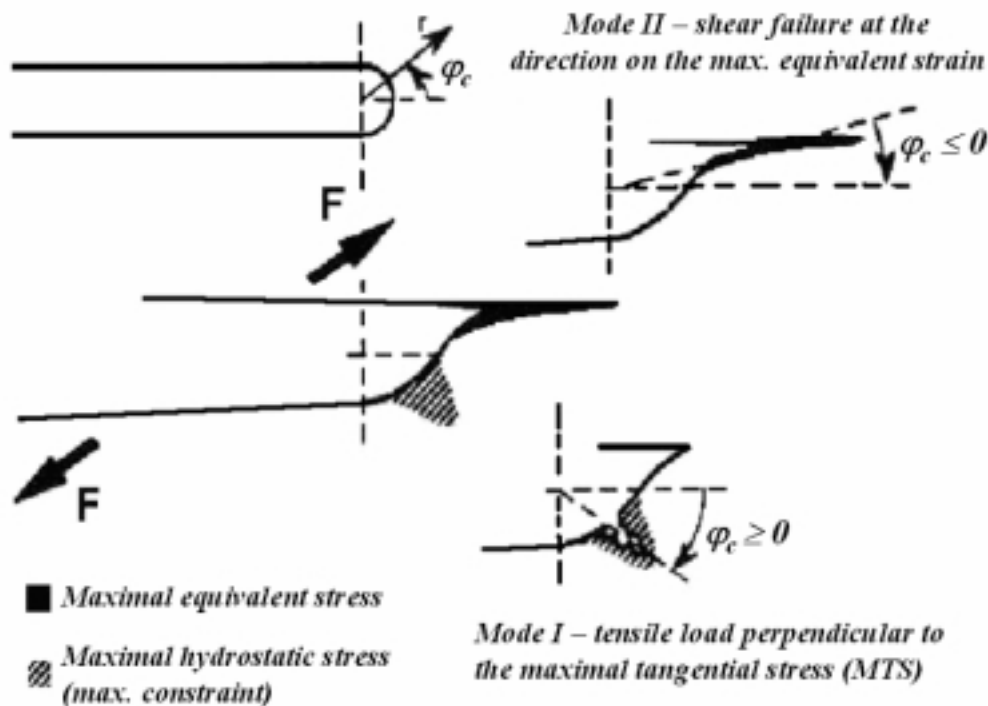


Figure 2.13. Asymmetric crack tip deformation due to high hydrostatic stresses and shear strains [27]

Beside opening or shear crack growth, there is a third class of crack growth usually observed in thin sheets: the slant (45°) crack growth. It takes normally place in isotropic, homogeneous thin-sheets principally under elastic conditions [7, 23].

The reason for slant growth may be related to the conditions for which a shear lip develops. Shear lip describes the shear deformation produced at the plate surfaces. In thick specimens, the creation of shear lips is attributed to buckling effects (severe out-of plane deformation) and they appear on both sides of the specimen approximately at the same time. Shear lip is also explained as an instability effect combined with creep or work hardening [16].

If the sheet is sufficiently thin the shear lips on the sides may joint together as represented at the bottom of Figure 2.14.a.

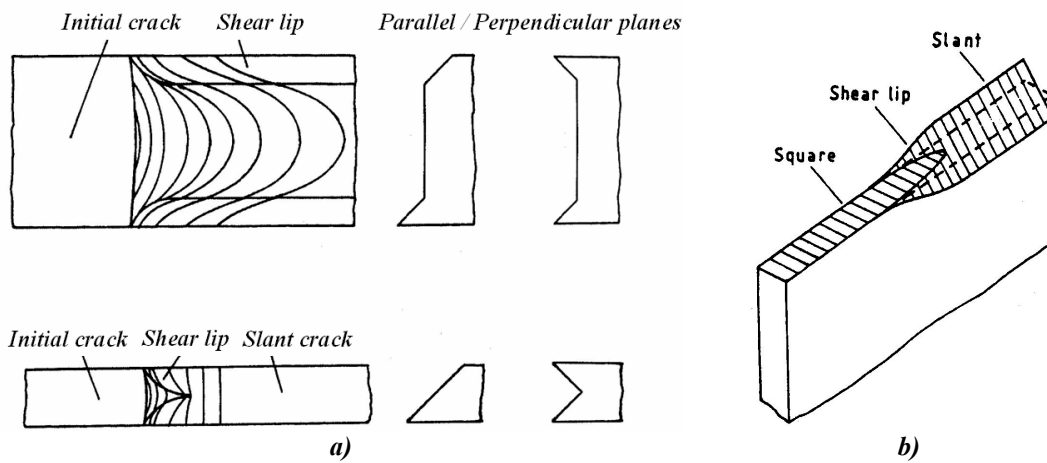


Figure 2.14. Transition to slant crack growth under a) static loading and b) cyclic loading [16]

In thick specimens, shear lips appear randomly on parallel and perpendicular planes, whereas in thin specimens they usually, but not invariably appear on parallel planes as represented in Figure 2.14. Some tests on 2 mm thick mild steel specimens performed by Ritchie [60], showed that the transition from plane crack to slant crack took place only when single edge notch specimens were loaded under tension, but not when they were loaded under three point bending. This observation suggests that the T -stress is a significant factor for the development of shear lip, and therefore a slant crack [16].

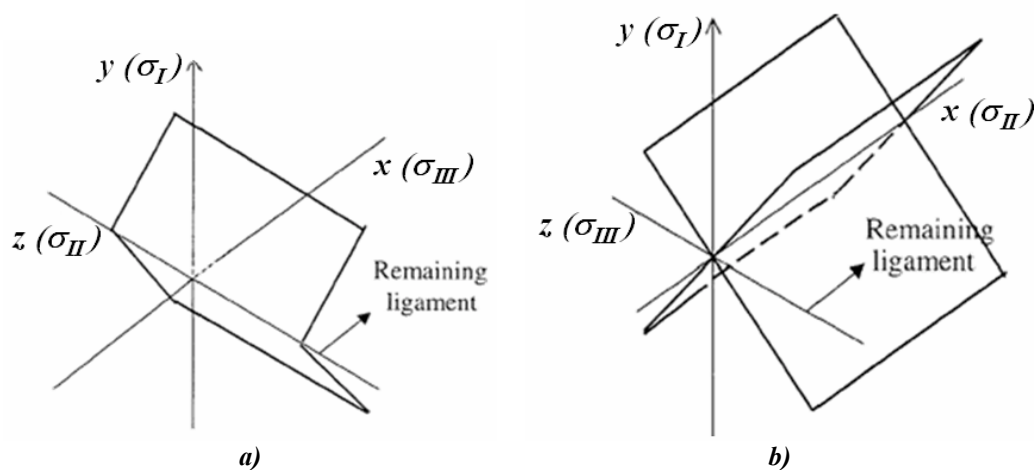


Figure 2.15. Fracture surface separation for a) plane strain and b) plane stress [61]

In order to explain the transition from flat to slant fracture, it should be recalled that the appearance of the crack surface is related to the principal stresses in plane strain and plane stress

conditions. For a symmetrical specimen pre-cracked in the plane xz , as represented in Figure 2.15, the principal stresses σ_I corresponds to the applied stress σ_y .

Under plane strain conditions ε_{II} is 0 and σ_{II} can only be produced by the Poisson's effect due to σ_{III} and σ_I . Therefore, σ_{II} corresponds to the thickness direction (σ_z) and σ_{III} to σ_x . Under these conditions the maximum shear stress acts along the planes at 45° from the z -axis, after Mohr. As a result, the fracture surfaces separate along the plane of the x -axis and retain the original crack plane.

Under plane stress conditions $\sigma_z = 0$ which matches with the lower principal stress, i.e. σ_{III} and then σ_{II} is equal to σ_x . Under these conditions, the maximum shear stress acts along the planes at 45° from the x -axis and the fracture surfaces tend to be parallel with the plane of maximum shear stress generating the slant crack [61]. In the above discussion σ_I is per definition larger than σ_{II} and this is larger than σ_{III} .

For the determination of a crack path, a criterion for crack growth and path direction is required. This criterion should be based on a parameter, which characterises stresses or displacements, or both, in the vicinity of a crack tip.

Because the principal challenge of this work is a study to perform crack turning assessment on a simple way, and because aeronautical structures are supposed to be loaded below the yield strength, it was decided to restrict this work to the linear elastic fracture mechanics domain. Besides, most of the existing criteria, for predicting crack turning under cyclic and/or quasi-static loading have been also developed on the *LEFM*-field.

Sections 2.4.2 and 2.4.3 explore the more representative criteria found in the literature for both mixed mode and *Mode I* loading. They are classified depending on their capability to assess crack turning on *2D*- and *3D*-structures loaded under mixed mode or under *Mode I*.

2.4.2 Crack turning criteria for 2D-structures

The more used criteria for *2D*-structures loaded under mixed mode are the maximum tangential stress, the maximum hoop stress (*MHSC*), the maximum energy release rate, and the stationary

Sih energy density factor criteria. However, it is found that the assessed crack paths using these different criteria are equivalent [23]. Therefore, the more representative of them is described below. The other criteria are described in the annexes, chapter A.2.1.

In 1963, Erdogan & Sih [62] observed that brittle materials under plane loading (*Mode I + II*), crack extension takes place in an angle $\varphi_c = 70^\circ$ from the plane of the crack. They found that this angle corresponds to the perpendicular direction to the maximal tangential stress evaluated at the crack tip, which is 70.5° . Besides, they noticed that this maximum coincides with a zero of the shear stress as illustrated in Figure 2.16.

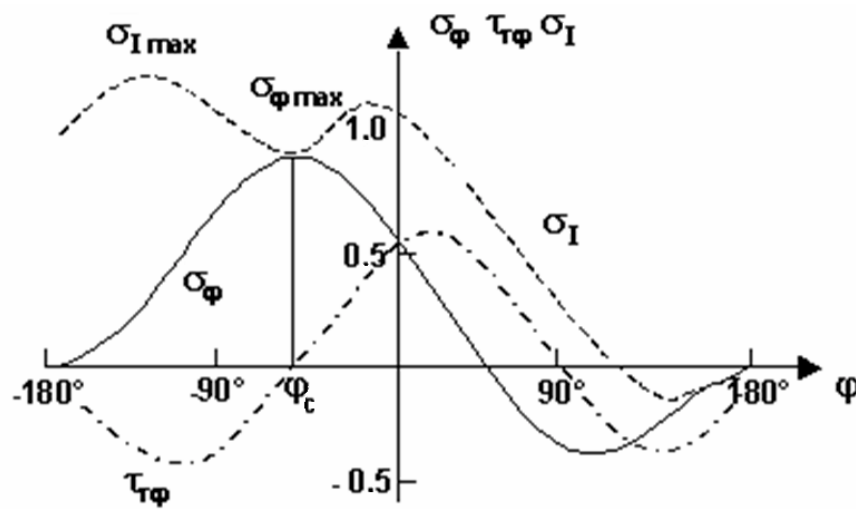


Figure 2.16. Development of the observed stresses by Erdogan & Sih [62]

Based on these observations, the crack turning angle of a straight crack in an infinite thin plate with ideally brittle behaviour can be determined. Based on the *LEFM* hypotheses and imposing the shear stress to be zero equation 2.4.1 is obtained.

$$\frac{K_{II}}{K_I} = \frac{-\sin \varphi_c}{(3 \cos \varphi_c - 1)} \quad (2.4.1)$$

Because the turning is predicted to be perpendicular to the maximum tangential stress, this criterion is called the maximum tangential stress criterion (*MTS*) [23].

Figure 2.17 depicts the crack path produced on a narrow body fuselage panel test and the crack path assessed after the *MTS*-criterion. Furthermore, different authors [9, 31] provided crack

turning data for *Al*-alloys and showed that there was good correlation with the *MTS*-criterion, at least in the predominant *Mode I* regime. They also noticed that under elastic plastic conditions the *MTS*-criterion left good assessment too, but only when fracture is tensile dominated.

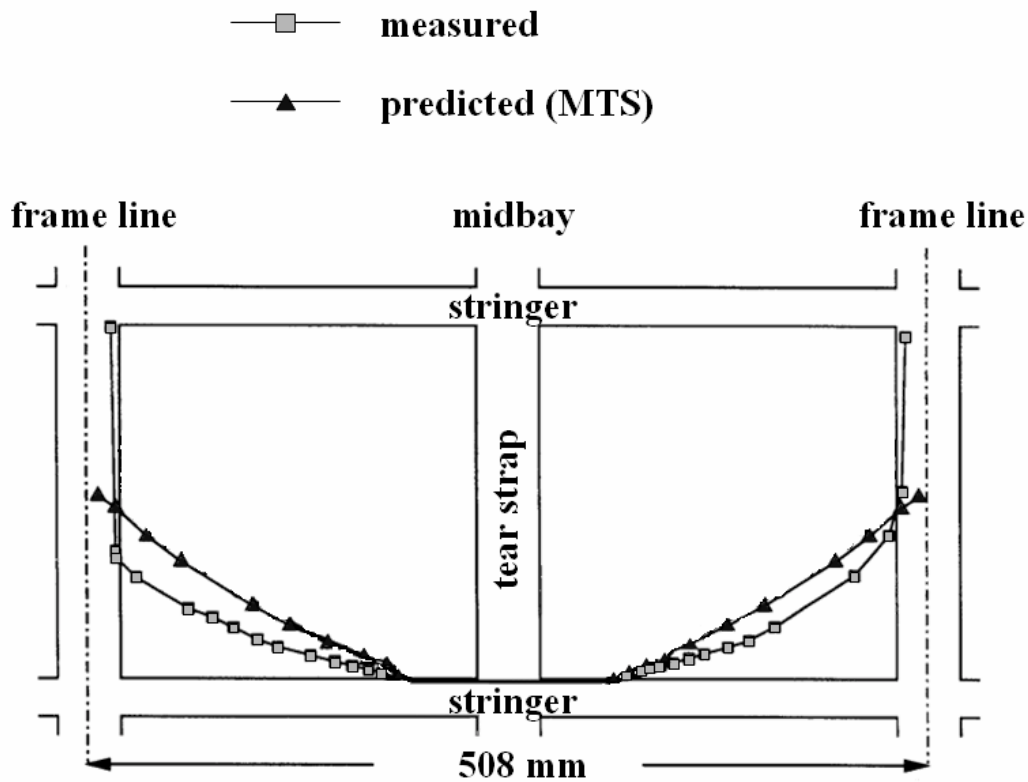


Figure 2.17. Experimental and assessed crack path on a narrow body fuselage panel test after the *MTS*-criterion [9]

As already explained in chapter 2.2.4, crack turning under *Mode I* loading is connected with strain localisation taking place at some distance from the crack tip. Therefore the stress field characterisation needs the second order term on the William's expansion series. Following, the criteria using this term are introduced.

Cotterell & Rice [63] proved that for a crack propagating under pure *Mode I*, the strain energy release rate is locally maximized for a straight crack extension. Thus, once a turn is established, the crack opens so that the displacements near the tip are proportional to the square root of the distance from the tip. This statement let to relate the energy release rate in terms of the *SIF*.

$$G_e = \frac{1-\nu^2}{E} [K_I^2 + K_{II}^2] \quad (2.4.2)$$

This relation is known as Irwin's expression.

The energy release rate was observed to be stationary with respect to the angle of the propagating crack, which implies that K_{II} should be zero. Supposing that the crack path can be represented as Figure 2.18, Cotterell & Rice described the stress intensity factor at the new extending crack, K_{II} , by means of equation 2.4.3.

$$K_{II} = k_{II} + \frac{1}{2} \lambda'(l) k_I - \sqrt{\frac{2}{\pi}} T \int_0^l \frac{\lambda'(l)}{\sqrt{l-x}} dx \quad (2.4.3)$$

where k_{II} and k_I are the *SIF* on *Mode I* and *II* respectively for the crack length before turning, T is the *T*-stress and $\lambda(l)$ and x are defined in Figure 2.18.

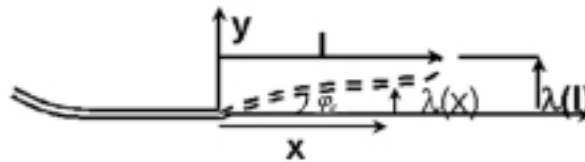


Figure 2.18. Crack path turning parameters

This equation can be used to calculate $\lambda(l)$ for crack paths with tangent angles lying within 15° on either side of the prolongation of the crack imposing that $K_{II} = 0$ at the crack tip of the extending crack.

Gao [35] carried out perturbation analysis for slightly non-planar half plane cracks to extend *2D* crack stability analysis of Cotterell & Rice to a *3D*-regime. It was found that while the stability of the crack against deflection in the *xy* plane is dominantly controlled by the *2D T*-component, the other two components, T_{zz} and T_{xz} , affect the stability against non-planar crack surface perturbations parallel to crack front, such as those leading to the so-called en-echelon crack front segmentation.

Sumi et al. [64] include one additional higher order term in the stress field expansion and proceed as Cotterell & Rice. This criterion showed that a large group of stable paths are misjudged using only the *T*-stress term as described in the annexes.

William and Ewing [65] proposed on the basis of the observations by Erdogan & Sih [62] that the crack would propagate in the direction of maximum tangential stress evaluated at a material specific distance, r_c , ahead of the crack tip. Finnie and Saith [66] and Kosai, Kobayashi and Ramulu [4] derived a more general formulation forcing the function of the tangential stress to have a maximum at $r = r_c$. With this, they obtained the implicit equation 2.4.4. This criterion is called from now on the *WEF*-criterion.

$$\frac{K_{II}}{K_I} = \frac{-2 \sin \frac{\varphi_c}{2}}{(3 \cos \varphi_c - 1)} \left[\cos \frac{\varphi_c}{2} - \frac{8T}{3K_I} \sqrt{2\pi r_c} \cos \varphi_c \right] \quad (2.4.4)$$

Observing equation 2.4.4 more in detail, it can be seen that the first order theory of Erdogan & Sih [62] is actually a special case of this. Making either $r_c = 0$ or $T = 0$, the equation 2.4.4 derives on equation 2.4.1.

When $K_{II} = 0$, there are two possible turn angles which satisfy equation 2.4.4. One angle is $\varphi = 0$ which results in a straight crack growth. Analysing the limit of the straight crack growth under pure *Mode I*, i.e. with $\varphi = 0$ and $K_{II} = 0$, the solution limit of the maximal tangential stress, can be calculated with equations 2.4.5.a and 2.4.5.b.

$$\frac{d\sigma_\varphi}{d\varphi} = 0 \quad \text{and} \quad \left. \frac{d^2\sigma_\varphi}{d\varphi^2} \right|_{\varphi=0} = 0 \quad (2.4.5.a) \text{ and } (2.4.5.b)$$

The solution of the above equations gives relation 2.4.6.

$$r = \frac{9}{128\pi} \left(\frac{K_I}{T} \right)^2 \quad (2.4.6)$$

Because the obtained r in equation 2.4.6 is an explicit solution, it is from now on defined as r_0 . Moreover, it was observed that when r_c is higher than r_0 , the angle solution $\varphi = 0$ is a minimum, and therefore the solution of the maximal tangential stress in equation 2.4.4 is a maximum for the non-zero angle solution. In other words the crack will turn. Crack turning will then occur, when both the T -stress is positive, $T > 0$, and r_c is higher than r_0 ($r_c > r_0$).

Figure 2.19 depicts the crack path produced on a narrow body fuselage panel test and the crack path assessed after the *WEF*-criterion with $r_c = 2.286$ mm.

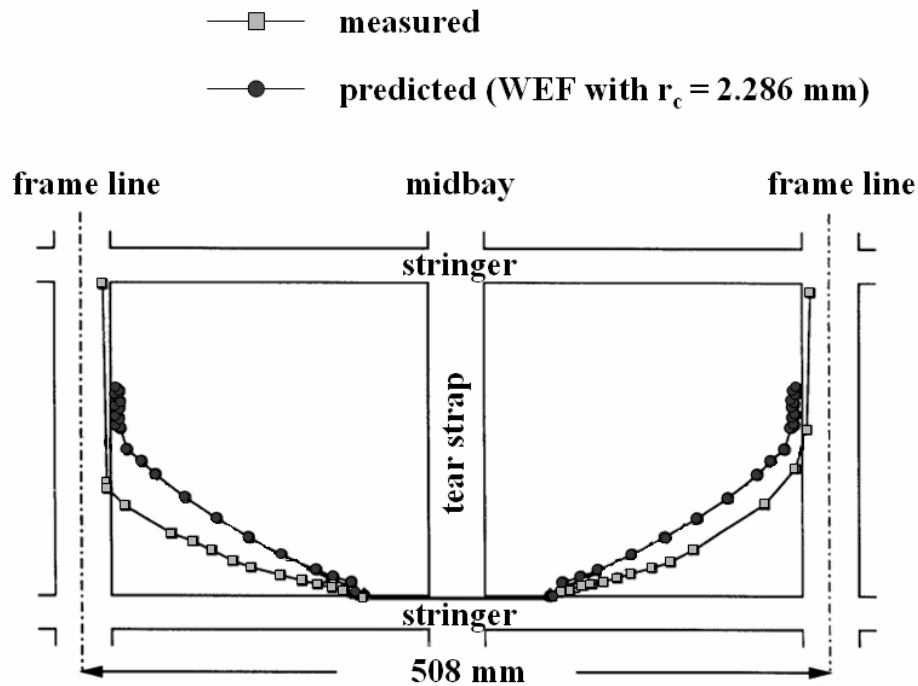


Figure 2.19. Experimental and assessed crack path on a narrow body fuselage panel test after the *WEF*-criterion [9]

Because the crack turns when $r_c > r_0$, the determination of r_c is of crucial importance. In the literature following r_c definitions and values are found.

a) Irwin [20] and Dugdale [67] developed approximate expressions for the size of the plastic zone in front of the crack tip in elastic-plastic materials. Reasoning that r_c is related to some failure process, it seems probable that the characteristic length associated with the maximum tangential stress crack turning theory should be no larger than the identified inelastic zones. Rice and Johnson [68] described r_c as the distance at which void growth or crack initiation will occur. Using values of strength and toughness, they evaluated r_c to be about 0.7 times the size of the plane strain's Irwin plastic zone radius.

b) Kosai [3], based on measurements of crack branches on the flanks of rapid fractures, estimated that for aluminium alloys 2024-T3 and 7075-T6, r_c was on the order of 1.53 mm.

c) For stable tearing, r_c was proposed to be determined by plotting the average of minimum turning radius as a function of r_0 [8], equation 2.4.6 and extrapolate the r_0 value at which crack turning occurs with zero radius. With this method, Pettit [23] found the critical value of r_0 , i.e. r_c , to be 1.27 mm for 2024-T3.

d) Chen [6] used a r_c value of 2.28 mm to obtain improved correlation between simulation and test results on a Double Cantilever Beam specimen of 2024-T3.

e) Streit and Finnie [69] determined r_c for 7075-T651 aluminium plates to be 2.54 mm using photo-elastic methods. With this method they observed the onset of path instability in symmetric specimens.

f) McMeeking and Parks [70] have shown, using a large deformation analysis, that the maximum stress occurs for materials with moderate strain hardening at a distance approximately given by:

$$r_c \approx \frac{J}{R_{p0.2}} \quad (2.4.7)$$

g) Defining $\sigma_T = T - \sigma^\infty$, where σ^∞ is the far field stress normal to the crack, when σ_T approaches the ultimate tensile strength of the material, R_m , the crack cannot continue to propagate along a straight path, and the panel must fail approximately perpendicular to the crack. This is because under these conditions σ_T becomes the maximal stress. Presumably this failure will show up as a bifurcating or turning crack. While a perturbed crack may well turn at lower transverse stress levels, even a perfectly unperturbed propagating crack must turn as σ_T approaches R_m . Thus, it does not seem unreasonable to consider the ratio K_c/R_m as a first approximation of the critical ratio of K_I/T at which crack turning must occur for unperturbed cracks [23]. Equating this to the bifurcation point in the 2nd order theory, r_c can be calculated as:

$$r_c = \frac{9}{128\pi} \left(\frac{K_c}{R_m} \right)^2 \quad (2.4.8)$$

For aluminium alloys ranging from $66.1-176.3 \text{ MPa}\cdot\text{m}^{1/2}$ plain stress fracture toughness and $408-612 \text{ MPa}$ ultimate strength, this gives r_c -values between 0.254 mm for brittle high strength alloys to 4.064 mm for low strength, very tough alloys [23].

If the crack is propagating at low SIF , the equivalent to K_c is the maximum cyclic stress intensity factor, K_{max} , which in slow crack growth range is typically an order of magnitude less than the fracture toughness. Thus, the characteristic length for cyclic loading crack, r_{cf} , can be evaluated with:

$$r_{cf} = r_c \left(\frac{K_{max}}{K_c} \right)^2 \quad (2.4.9)$$

r_{cf} will change into the constant r_c value as the applied stress intensity factor approaches K_c [8, 9, 23, 49].

Table 2.4 summarises the different definition and values for r_c found in the literature.

Table 2.4. r_c literature values

Data	r_c [mm]	Definition	Material
Rice & Johnson [68]	$0.7r_p$	Where void growth or crack initiation will occur	Ductile
Kosai [3]	1.53	Measurements of crack branches on the flanks of rapid fractures	AA 2024-T3 and AA 7075-T6
Pettit [8, 23]	1.27	Plot φ_c as a function of r_0 , and extrapolate r_0 for a $\varphi_c = 0$	AA 2024-T3
Chen [6]	2.28	Simulation correlation	AA 2024-T3
Streit & Finnie [69]	2.54	Using photo-elastic methods to observe the onset of path instability in symmetric specimens	AA 7075-T6
Pettit [23]	0.254-4.064	Assuming that the panel fails perpendicular to the crack \rightarrow when σ_T approaches R_m .	Brittle-ductile

Experimental tests show that on rolled sheet and plate products, the crack growth resistance has its maximum when the crack cross the rolling direction ($90^\circ/L-T$) and its minimum when the crack growth parallel to the rolling direction ($0^\circ/T-L$). Due to the fact that crack propagation and crack turning behave different depending on the propagation direction relative to the rolling direction, Buczek & Herakovich [71] and Boone [72] proposed a second order theory for materials with fracture anisotropy.

$$K_c(\varphi)^{n_0} \left(\frac{\cos^2 \varphi}{K_c(0^\circ)^{n_0}} + \frac{\sin^2 \varphi}{K_c(90^\circ)^{n_0}} \right) = 1 \quad (2.4.10)$$

The crack growth resistance, which is dependent on the angle produced between the crack and the rolling direction, φ , was approximated as an elliptical function as depicted in Figure 2.20 and described in equation 2.4.10.

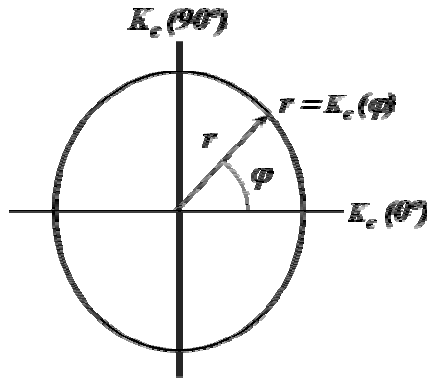


Figure 2.20. Schematic orthotropic crack growth resistance

n_0 is a constant exponent, which for most materials has the value of 2. For fatigue crack growth, K_c represents the *SIF* at which the crack propagates at a given rate, and for stable tearing, K_c represents the fracture toughness. Defining the fracture anisotropy as the ratio of the transverse crack growth resistance to the longitudinal crack growth resistance, equation 2.4.11, Buczek & Herakovich [71] suggested that the crack path in anisotropic materials would follow the maximum of the ratio of the tangential stress to the crack growth resistance.

$$K_m(\varphi) = \frac{K_c(90^\circ)}{K_c(0^\circ)} = \frac{K_{cL-T}}{K_{cT-L}} \quad (2.4.11)$$

Maximizing the ratio of the tangential stress to the crack growth resistance and separating variables equation 2.4.12 is obtained.

$$\bar{T} = \frac{\sin \varphi_c + \frac{K_{II}}{K_I} (3 \cos \varphi_c - 1) - 2 \Psi_I \left[\frac{K_{II}}{K_I} \sin \varphi_c - \frac{1}{3} (1 + \cos \varphi_c) \right]}{\sin \left(\frac{\varphi_c}{2} \right) (2 \cos \varphi_c - \Psi_I \sin \varphi_c)} \quad (2.4.12)$$

where $\Psi(\varphi + \varphi_c) = \left(\frac{2}{n_0}\right) \frac{\beta_m \sin 2(\varphi + \varphi_c)}{1 + \beta_m \cos 2(\varphi + \varphi_c)}$ (2.4.12.a) and Ψ_I is Ψ referenced to the *Mode I*

anisotropy ratio K_{Im} and $\beta_m = \frac{K_m^{n_0} - 1}{K_m^{n_0} + 1}$ (2.4.12.b).

Figure 2.21 depicts the crack path produced on a narrow body fuselage panel test and the crack path assessed after the *WEF* combined with the fracture anisotropy criterion, from now on *WEFO*.

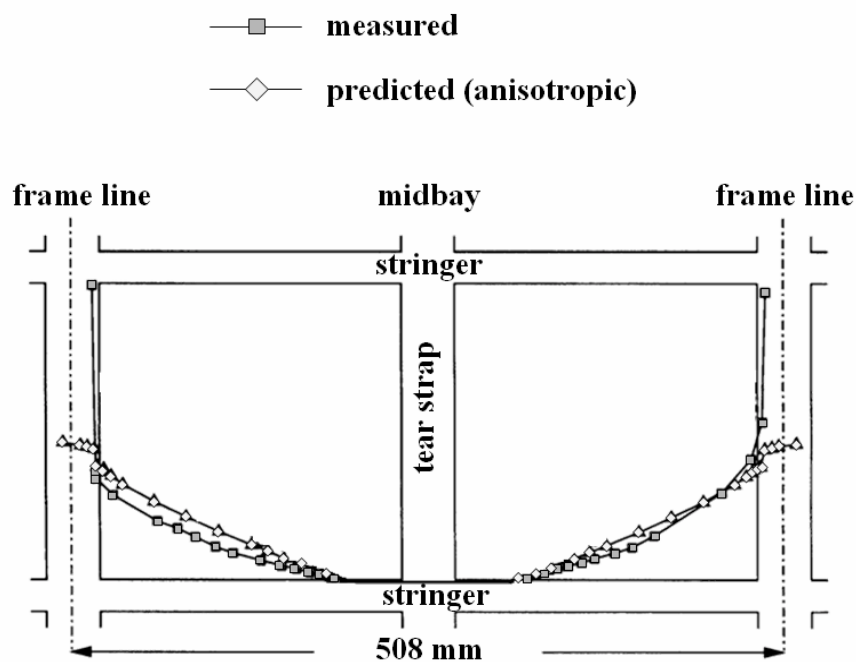


Figure 2.21. Experimental and assessed crack path on a narrow body fuselage panel test after the *WEFO*-criterion [9]

2.4.3 Crack turning criteria for 3D-structures

The criteria able to describe the crack path on 3D-structures are developed from 2D-criteria, based on experimental data or developed from new hypotheses. The two more representative are described here; other criteria are described in the annexes.

Sih [73] proposed that the crack path will grow in the direction of the minimal energy density defined as a function of the stress intensity factors. To find the turning and twisting angles, φ_c

and ψ_c respectively, the energy density must be minimized. It is found that φ_c is dependent on ν , *Mode I* and *Mode II* stress intensity factors, but independent on ψ_c and K_{III} . The minimum of the energy density was found to be always in the direction of “ $\psi = 0$ ” independently on the mixed mode combination. Hence, this criterion has to be regarded insensitive to K_{III} [22].

Based on experimental results, Richard [22] defined the crack turning and twisting angles as:

$$\varphi_c = \mp \left[R_1 \frac{|K_{II}|}{K_I + |K_{II}| + |K_{III}|} + R_2 \left(\frac{|K_{II}|}{K_I + |K_{II}| + |K_{III}|} \right)^2 \right] \quad (2.4.13)$$

φ_c is defined negative for $K_{II} > 0$ and positive for $K_{II} < 0$ and $K_I \geq 0$, and

$$\psi_c = \mp \left[R_3 \frac{|K_{II}|}{K_I + |K_{II}| + |K_{III}|} + R_4 \left(\frac{|K_{II}|}{K_I + |K_{II}| + |K_{III}|} \right)^2 \right] \quad (2.4.14)$$

If $K_I \geq 0$, ψ_c is defined as negative when $K_{III} > 0$ and positive when $K_{III} < 0$. On the basis of experimental tests for different static mixed mode ratios, Richard found the constants defined on equations 2.4.13 and 2.4.14, i.e. R_1 , R_2 , R_3 and R_4 , to be 155.5° , -83.4° , 78° and -33° respectively. Under cyclic mixed loading the crack turns more suavely than under static loading, therefore Richard applied the values of R_1 , R_2 to be 104.9° and -80.4° respectively obtaining a better adjustment with experimental results.

The fracture limit surface for spatial mixed mode loading was also defined based on experimental results as:

$$K_v = \frac{K_I}{2} + \frac{1}{2} \sqrt{K_I^2 + 4(\alpha_1 K_{II})^2 + 4(\alpha_2 K_{III})^2} = K_{Ic} \quad (2.4.15)$$

where $\alpha_1 = K_{Ic}/K_{IIc}$ and $\alpha_2 = K_{Ic}/K_{IIIc}$. Taking $\alpha_1 = 1.155$ and $\alpha_2 = 1.0$ the fracture limit surface is nearly identical to the surface defined on the maximum circumferential stress criterion. Richard proposed that the stress intensity factor at the turned crack tip, K_I , can be calculated with the equation 2.4.15 by applying $K_I = K_v$.

2.4.4 Summary of crack turning criteria

All criteria agree that the sign of φ_c is dependent on the sign of stress intensity factor under *Mode II*, K_{II} , as well as on the sign of the shear stress, τ_{xy} , as represented in Figure 2.22. Moreover, the initial direction of the branch crack follows the path, which decreases K_{II} to zero. This approach is related to the critical plane fatigue criteria [74].

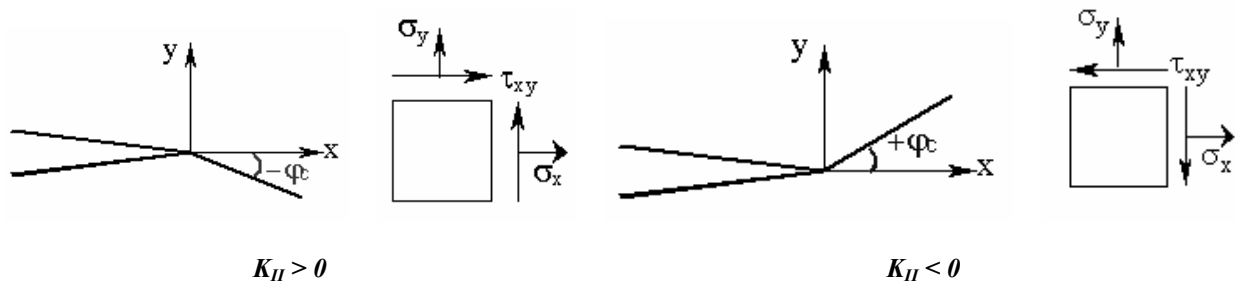


Figure 2.22. Sign of the angle depending on K_{II} , i.e. τ_{xy}

Studies on different crack turning criteria demonstrate that the *MHSC* and *MTS* conduct to the same path predictions. Moreover, Maiti and Smith (1983) [75] demonstrated that the observations done by Griffith [76] implies that the crack must propagate perpendicular to the stress load, which agrees with the maximum principal stress criterion [59].

One of the advantages using second order criteria is the prediction of a higher angle compared with first order criteria. However, one of the disturbing things, for example in the *WEF*-criterion and particularly in the case of stably tearing cracks, is that the applicable plastic zone sizes are typically substantially larger than the values obtained for r_c . Thus, the linear elastic basis of all formulations is known to be invalid. Nevertheless, a good reliability was obtained when comparing experimental crack turning results and crack path predictions using this criterion. Therefore, it can be assumed that linear elastic theory may adequately predict the turning angle under large deformations.

2.5 Crack growth on fuselages

Commonly, failures in engineering components are associated with stress concentrations resulting from design errors, e.g. the presence of holes, notches, tight fillet radii, voids and/or inclusions on the microstructure, and corrosive attack. Table 2.5 gives an overview on the

percentage of failure mechanism produced on engineering and aircraft components. It can be seen that in aircraft incidents, the cause of failure is dominated by fatigue failure in a 55% of the cases.

Table 2.5. Frequency of failure mechanisms

	<i>Percentage of failures</i>	
	<i>Engineering components</i>	<i>Aircraft components</i>
<i>Corrosion</i>	29	16
<i>Fatigue</i>	25	55
<i>Brittle fracture</i>	16	-
<i>Overload</i>	11	14
<i>High temperature corrosion</i>	7	2
<i>Stress Corrosion Crack/Corrosion Fatigue/Hydrogen Embrittlement</i>	6	7
<i>Creep</i>	3	-
<i>Wear/abrasion/erosion</i>	3	6

At the beginning of the aircraft industry, stress engineers certified the structures evaluating only their maximal loading capabilities, i.e. only based on static structure behaviour. Fatigue life and multi-site damage (*MSD*) analyses were firstly introduced to the safety program validation due to catastrophic disasters; on the Comet transport jet aircraft (1954) and the Aloha flight 243 (1988) respectively, illustrated in Figure 2.23.



Figure 2.23. Failure of a) Comet transport jet aircraft from fatigue. b) Aloha Flight 243 in which the airplane lost a large section of its upper fuselage due to MSD

Nowadays, it is generally recognised that the design of a structure of commercial aircraft (*A/C*) cannot be considered to be complete without fatigue analysis. Furthermore, the investigation of defects and failures during service are of vital importance to prevent incidents [1, 77, 78].

2.5.1 Load on aircraft structures

A fuselage is loaded by internal pressure, which produces the shell to move outward in radial direction. The restriction of this movement, due to the structure configuration, causes a hoop stress in the skin. The frames and the stringers restrain partially the outward movement causing non-uniform membrane stress distribution and bending stresses around them. The fuselage is also loaded with an overall bending moment as a result of the aircraft lifting, which takes place at the wing level. The hoop stress and the bending moment cause biaxiality ratios, which change across the circumference of the fuselage. Additionally, side panels are loaded by a shear force creating shear stresses.

Frames, stringers, crack stoppers or tear straps do not only restrict the outward movement produced by the internal pressure but they limit the stress intensity factor in a cracked skin. In unstiffened panels with a crack propagating, the *SIF* increases until the crack reaches a critical length and fast fracture occurs, yielding to the complete failure of the panel. A redistribution of the load on the skin is produced with the presence of the stiffening elements transferring a large portion of the skin loads to them, and so reducing the *SIF*. Therefore, the hoop stress is significantly reduced as a longitudinal crack approaches a frame, due to the load transfer from the skin to the frame [24, 79]. Moreover, in differential structures, stiffening elements are attached mainly due to their axial stiffness. When the crack crosses the stiffening element without damaging it, it provides a flexible bridge across the crack and it limits the amount of crack opening and the quantity of crack propagation [80].

Carefully designed frames with circumferential crack stopper straps confine the damage in a local area. In stiffened panels, a greater reduction in stress could be expected with increasing stiffener area if the centre stiffeners were assumed to be intact. The effect of stiffener elements on the stress intensity factor in redundant, built-up structures can be expressed as a function of geometrical effects, i.e. stiffener spacing, stiffener section properties, area, inertia, neutral axis location, material properties (elastic or plastic), fastener displacement (linear or non-linear), skin thickness, Young modulus, Poisson's ratio and of course geometry and crack length [5, 8]. All these properties are characterized by the geometric factor on the calculation of the stress intensity factor [1, 27, 77, 78].

Due to the importance of the stiffening elements, a large number of studies on the design of these reinforcements have already been carried out regarding the improvement of damage tolerance. It was found out that the residual strength decrease when increasing stiffener spacing, decreasing the stiffener area or increasing rivets spacing. Besides, it was also observed that an augmentation on the stiffener strength produces only a slight improvement of the residual strength [9, 13, 23, 24, 81-83].

2.5.2 Crack turning on fuselages

Crack stoppers and tear straps are principally designed to arrest longitudinal and axial cracks, respectively. But they encourage the crack to turn due to the generation of a complex stress field at the crack tip, which contains an in-plane shear mode loading. Consequently, the principal reason of this crack deflection is produced by the presence of K_{II} . Large crack turning generates a large axial stress ahead of the propagating crack tip and together with the reduced circumferential stress, as a result of the tear strap or the stringer, the turning is stabilised. After turning under these circumstances, the crack can propagate further under pure *Mode I*, if it has deviated away from the constraining effect of the longitudinal stringer, or the crack can be arrested, if the turning generates the flap of the upper skin [3, 82]. If flapping takes place on both sides of the crack, a large opening on the fuselage is generated and the crack driving force is reduced through the “controlled” depressurisation of the cabin as illustrated in Figure 2.24.

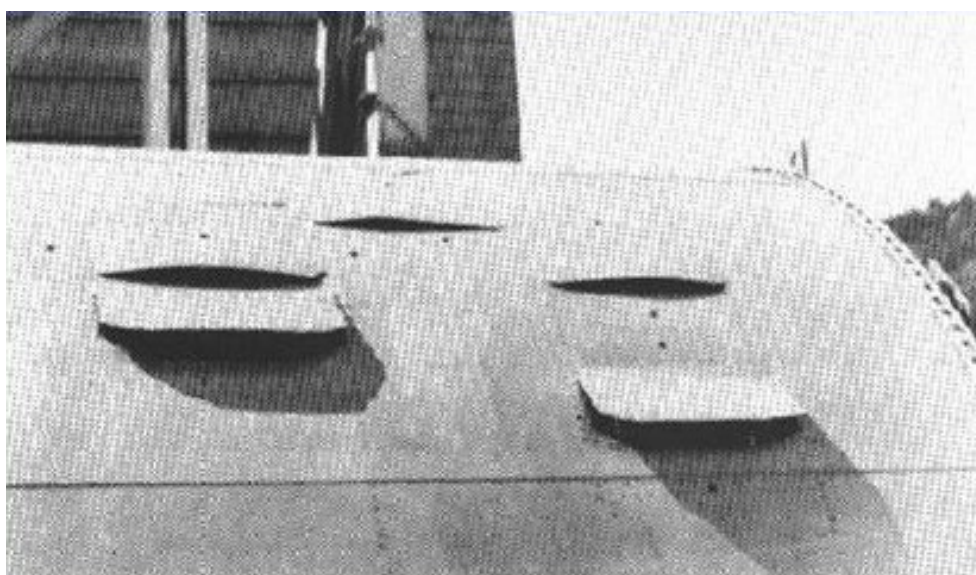


Figure 2.24. Crack turning and flapping in Boeing 707 barrel- test [8]

This flapping phenomenon has been pointed out by different authors when testing thin-sheet structures. Swift [2] perceived it in unstiffened cylinders. Kosai [3] observed it when analysing crack growth on a fuselage with bonded stiffeners. And Pettit [7] studied the crack turning and crack arrest in integrally stiffened fuselage with propagating transverse cracks.

However, for an airplane in flight, the high velocity airflow along the fuselage will tend to close the flap, and thus counteracting the effect of the opening flap due to the cabin pressure [4]. The net result is that the axial crack will continue to propagate. Although this statement, flapping is used as a fail-safe criterion on the Boeing 707, 727, and 737 fuselages for regions excluding the joint areas.

Crack turning on differential structures is also used to maintain a low level of inspection costs. A crack growing in the rear panel of a joint area can not be detected because its growing occurs in a non-visible zone. Thanks to crack turning the crack leaves the joint and becomes visible, as schematised in Figure 2.25.

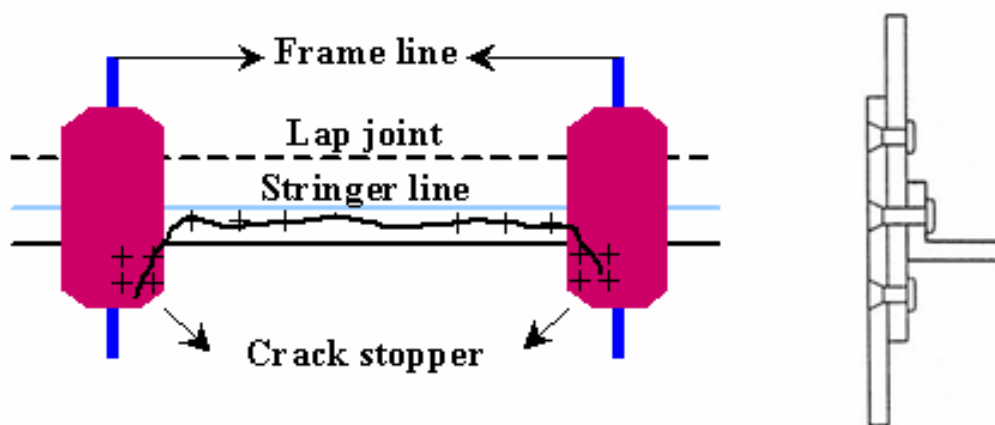


Figure 2.25. Schematic longitudinal crack in the Airbus A320 fuselage [24]

In this case the crack turning is known to be produced by the stress redistribution generated near the crack stopper. Although this is the last defence of an axially rupturing fuselage, not much is known about its effectiveness in arresting the crack. And much of the tear straps design is based on empirical rules derived from sub- and full-scale testing of pressurised fuselages.

Potyondy [84] was able to approximate the actual behaviour of the crack growing near the tear strap in the smoothly curved region using the maximal tangential stress criterion of Erdogan &

Sih. But the sharp turning radius observed as the crack grew parallel to the tear strap, resulting in flapping was not predictable. The work of Kosai [3] and Knops [85], among others authors, gave substantial evidence that to predict more accurately the crack turning in pressurized cylinders, a second-order criterion is needed. The criterion described by Finnie and Saith et al. [66] predicted that the crack would turn more sharply than the first order predictions. This improved the correlation with experimental results [9].

Different studies on aeronautical structures agree with the idea that crack turning can result from the presence of high T -stress. This stress develops as part of the non-linear response to internal pressurisation. Because the circumferential hoop stress is approximately twice the longitudinal bulge stress and due to bending, the produced biaxiality ratio at the crack tip increases in the top of the fuselage and decreases in the bottom. Consequently, the T -stress increases when moving to the top and decreases moving to the bottom. Therefore, crack path instability will become more probable on the top part of the fuselage and will be postponed into the bottom [80]. Furthermore, Zaal [24] proposed that on stiffener cylinders, the stiffening elements might have positive contribution to the T -stress and thus decrease the crack length at which the crack path becomes directionally unstable [78].

In order to understand and analyse this phenomena on a low cost, laboratory specimens are needed. To investigate the curved path under mixed mode loading, different specimens have been developed. It is the case of the transversal force bending specimen, developed by Theilig [86], or the compact tension shear (CTS) specimen by Richard [87]. This last one, in combination with a special loading device, have contributed to the current state in the field of mixed mode loading helping different authors to corroborate and develop mixed mode criteria by means of both experiments and simulations. But, there are two broadly used laboratory specimens that reproduce the load conditions on aircraft structures near *Mode I* loading. They are the DCB and the CFS . Positive T -stresses are generated on the DCB and the K_I/T -ratios are comparable to the ratios produced when the crack is situated on the region adjacent to stiffeners. On the CFS , the biaxiality ratio can be directly controlled by means of the stress parallel to the crack.

It is principally for these reasons that these two specimens have been selected to perform the most part of the analysis contained in this doctoral thesis.

2.5.3 The Double Cantilever Beam specimen

On the study of compact tension (*CT*) specimens, it was noticed that the *T*-stress varied with the crack length and its value became positive for a considerable range of crack propagation. Under these conditions, some second order criteria predict an unstable crack path, but in experimental tests the cracks never deviated from the symmetry line of the specimen. In order to transform this theoretical instability on real curved crack path, some modifications on the *CT*-specimen were carried out [53], for example as represented in Figure 2.26. However, in this example, a *Mode II* load appears as a result of the geometrical asymmetry, which is clearly the responsible of the curved path.

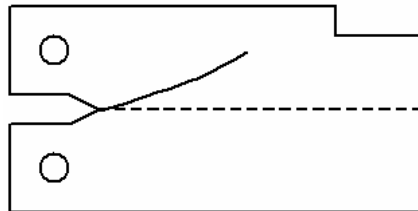


Figure 2.26. Asymmetrical *CT*-specimen [53]

Mostovoy [88] modified the *CT*-specimen manufacturing it with larger widths and with tapered forms. Experimental tests were carried out on these modified *CT*-specimens made of polymetacrylate of methyl and manufactured with different tapered angles, α_m in Figure 2.27. *CT*-specimens with larger width are called *DCB*-specimens and those including an angle are called tapered *DCB*-specimens.

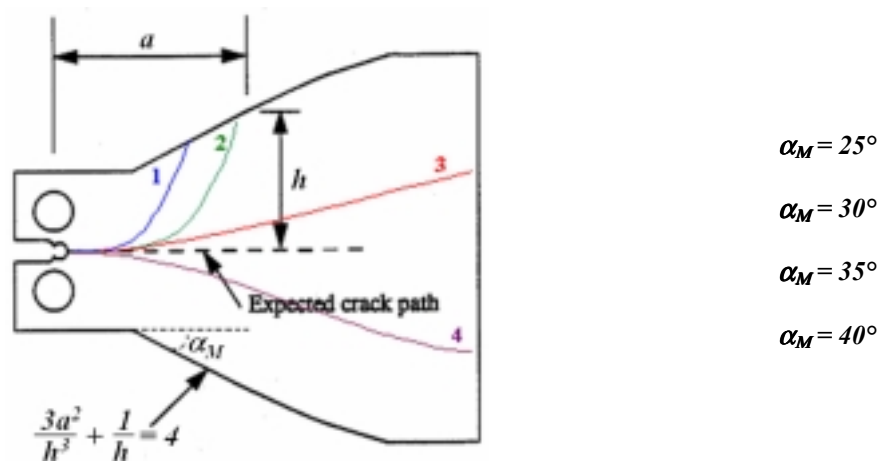


Figure 2.27. Mostovoy specimen. Different crack turning paths due to different tapered angles, α_M [88]

Swift [5] analysed rectangular *DCB*- and tapered *DCB*-specimens made of aluminium, with different tapered angles and crack length to width ratios. Different crack path trajectories were obtained as in the Mostovoy experiences [80].

A further modification of a *DCB*-specimen is the twist double cantilever beam (*SDCB*), performed by Pettit [7] and represented in Figure 2.28. This specimen presents two extra points of load introduction and it was developed in order to better determine the characteristic distance to the crack tip, r_c , for the crack turning assessment.

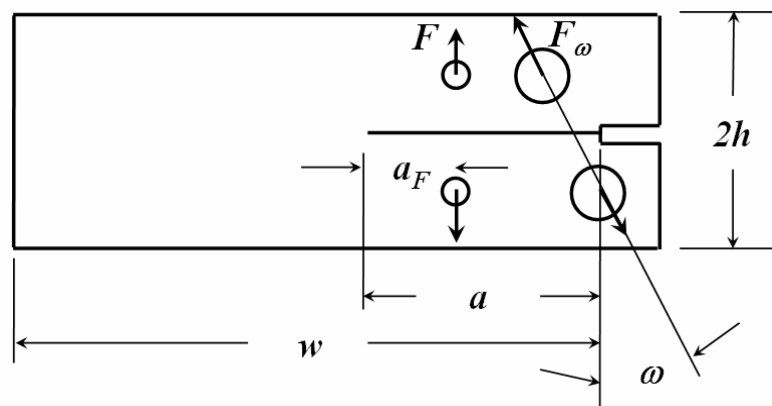


Figure 2.28. *SDCB*-specimen

2.5.4 The cruciform specimen

As a consequence of loading, geometry and/or material inhomogeneities, engineering structures are influenced by complex multiaxial stresses. However, standard laboratories testing uses principally simple specimens subjected to uniaxial states of stress in all kinds of loading regimes, e.g. creep, quasi-static and cyclic loading tests. Because of the divergence between design-based uniaxial test data and the functional operation of components, more and more research works are conducted to ensure that the relationship between the two is adequately understood. Furthermore, biaxial or triaxial test facilities have been created to understand better the superposition of multiaxial stresses.

Beside this, as already explained, the fuselage of an aircraft is loaded with a hoop stress and a bending moment which cause a varying biaxiality ratio across the circumference of the fuselage. This biaxiality ratio can be reproduced and analysed by means of cruciform specimens and the

correspondent test rig. The load in the y -direction, σ_y , simulates the hoop stress of the fuselage and the load parallel to the crack, $\lambda\sigma_y$, simulates the effect of bending moment as well as the large axial stress, which can be produced when the crack flaps. An unloading of the middle of the specimen is produced due to the deviation of the force flow introduced on the arms and the stress raise created at the specimen edge as illustrated in Figure 2.29.

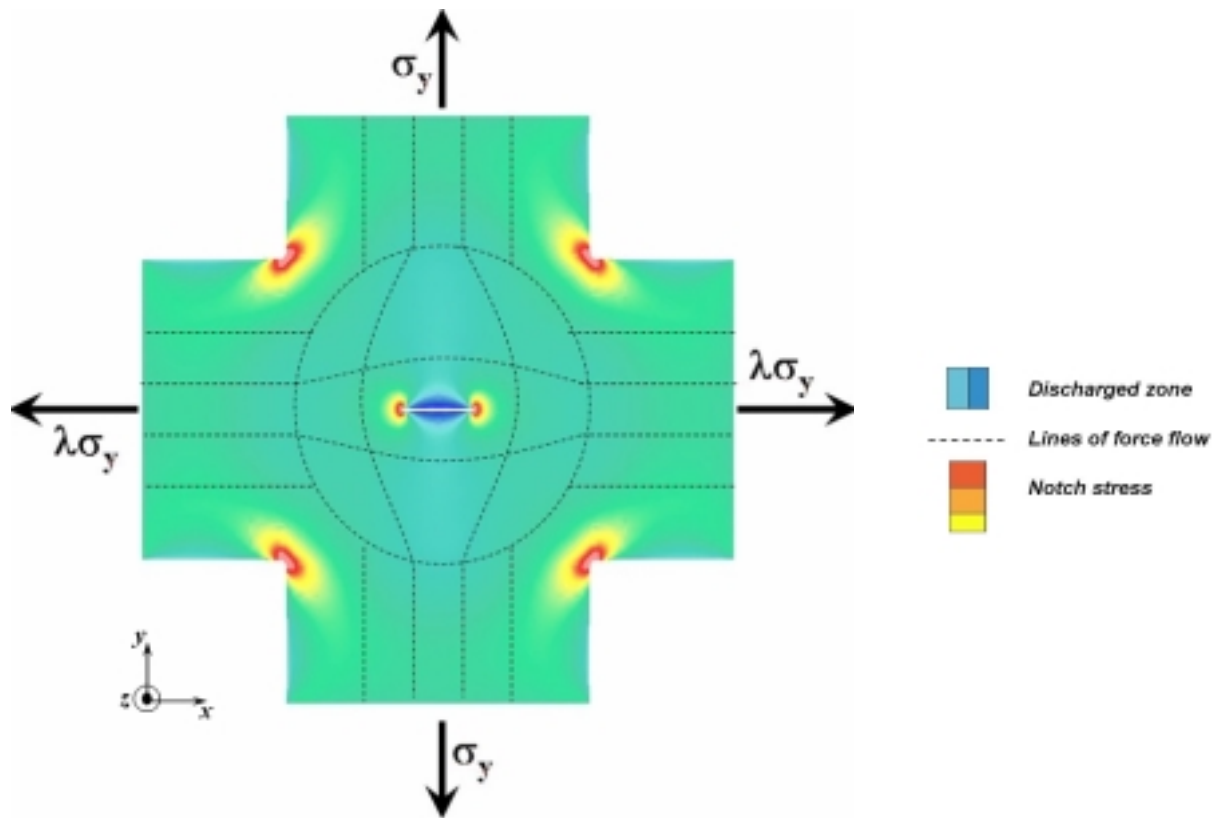


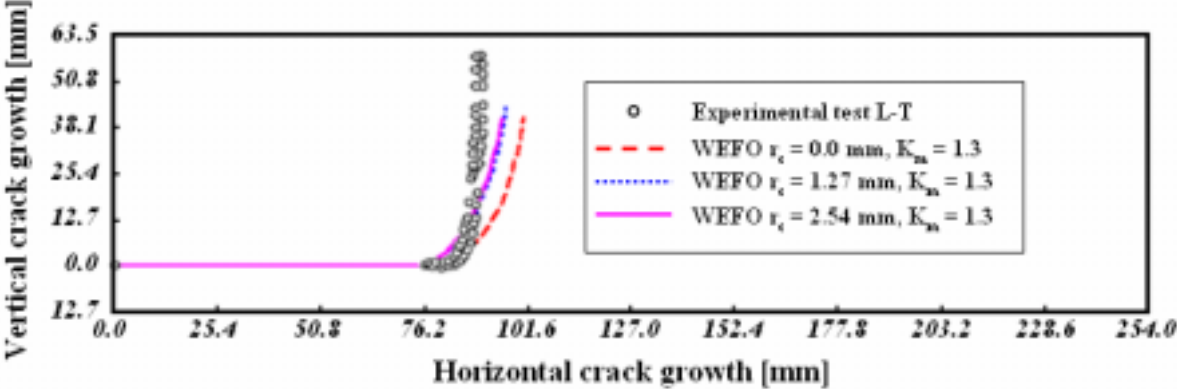
Figure 2.29. Stress flow on the CFS-specimen

As already pointed out, such test and specimen produce positive T -stress and it can be controlled by means of the loading in the y -direction, i.e. σ_y , and consequently control crack turning.

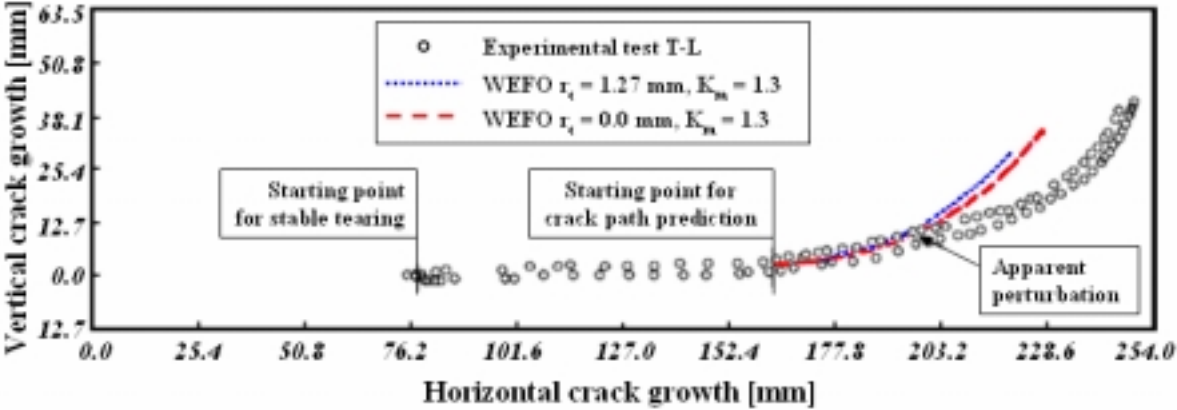
2.5.5 Assessment of crack turning on the DCB-specimen

The analyses dealing with the crack path prediction on DCB -specimens and found in the literature treat the problem as two dimensional and investigate the crack path by means of the criteria described on sections 2.4.2 and 2.4.3.

These analyses shown that the criteria that do not use higher order terms, i.e. the T -stress, can not predict any crack turning. The best assessment on the experimental crack path was achieved by means of the *WEFO*-criterion as illustrated in Figure 2.30.



a)



b)

Figure 2.30. Crack path assessment using the *WEFO*-criterion on DCB-specimen in a) L-T and b) T-L direction [23]

However, as can be seen in Figure 2.30.b, the prediction fails to determine the starting point of turning, and there is certain dependency on the selected r_c -value.

